ELECTRONIC SUPPLEMENTARY INFORMATION

A Robust, High-Sensitivity Stealth Probe for Peptidases

Oliver Thorn-Seshold, Monica Vargas-Sanchez, Sean McKeon and Jens Hasserodt*

* Laboratoire de Chimie, CNRS, École Normale Supérieure de Lyon, 46 Allée d'Italie, F-69364 Lyon, France.
E-mail : jens.hasserodt@ens-lyon.fr

Synthesis

General notes

Dry tetrahydrofuran (THF), toluene and dichloromethane (DCM) were obtained by passing commercially available pre-dried formulations through activated alumina columns under argon. Dry EtOH and pyridine were obtained by standing the commercial dry HPLC grade solvents for 24 h on thermally-activated molecular sieves (3Å, sieve activation by 24 h heating at 315°C). Column chromatography was performed on Merck silica gel Si-60 (40-63 μm). Unless stated otherwise, all reactions were performed with unpurified, undried, non-degassed solvents or analytical grade reagents, used as obtained, under closed air atmosphere. Procedures and yields are unoptimized.

All compounds have ^{1}H- and ^{13}C-NMR spectra fully assigned. Where necessary, HSQC, COSY and HMBC spectra were used to assign spectra. Raw ^{1}H-NMR and, where deemed necessary *e.g.* by reason of complicating signals from diastereomeric forms, ^{13}C-NMR spectra are given in the NMR Appendix; these are indicated where appropriate. All spectra were acquired on a Bruker DPX 200 (200 MHz & 50 MHz for ^{1}H and ^{13}C respectively) or on a Bruker AVANCE 500 (500 MHz & 125 MHz for ^{1}H and ^{13}C respectively) as indicated, at 300K. Chemical shifts (δ) are reported in ppm with reference to residual solvent signals; peaks are annotated as follows: s=singlet, d=doublet, t=triplet, m=multiplet, br=broad; coupling constants J are given in Hertz (Hz) and refer to (H,H) coupling unless otherwise specified; "~" indicates an apparent peakform, thus ~t denotes an apparent triplet, with its corresponding apparent coupling constant value given. Unit mass measurements were performed on an AGILENT 1100 SL coupled LC-MS system with direct injection of the sample in ESI mode. HRMS was carried out by the Service Central d'Analyse du CNRS, Solaize, France.

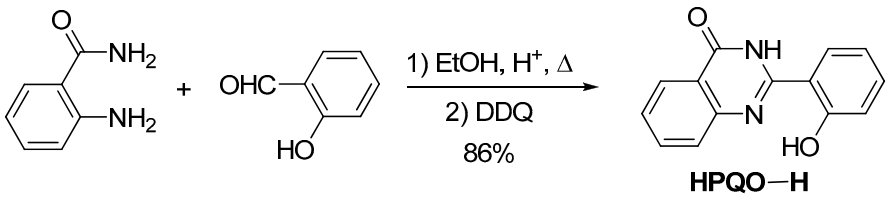

5 : 2-(2-hydroxyphenyl)quinazolin-4(3*H*)-one (HPQ / HPQO-H)

The following procedure was adapted from Waibel[S1]. To a solution of anthranilamide (1.60 g, 11.75 mmol) in absolute EtOH (30 mL) was added salicylaldehyde (1.44 g, 11.8 mmol) giving a yellow solution and a precipitate. The reaction was heated to 80°C under a condenser open to the air for 30 min, then *p*-TsOH monohydrate (43 mg, 0.22 mmol) was added and the precipitate dissolved. The solution was heated to 80°C for 1 h, then cooled to room temperature and DDQ (2.70 g, 11.8 mmol) was added. The mixture was stirred at RT, open to the air, overnight. The solid was filtered on a porosity 4 glass frit and air dried, rinsed twice with diethyl ether then dried at reduced pressure giving **HPQO-H** (2.4 g, 10 mmol, 86 %; referred to in the main article simply as HPQ) as a beige powder showing strong green fluorescence under a 365 nm UV lamp. **HPQO-H** has R_f = 0.56 in 1:1 Cy:EA and is stained by $KMnO_4$ but not by ninhydrin. NMR in d_6-DMSO matched data of Baghbanzadeh *et al*.[S2].

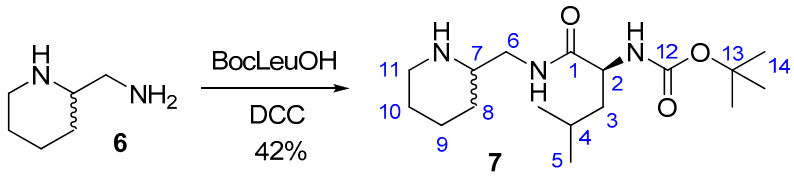

7 : (*N*'-*tert*-butoxycarbonyl)-L-leucyl-(piperidin-2-ylmethyl)amide

A DCC-mediated coupling gave the desired regioselectivity of N-acylation. BocLeuOH (4.385 g, 19.0 mmol) was dissolved in dry DCM (50 mL) before cooling in an icebath. DCC (3.95 g, 19.1 mmol) was added and the mixture stirred for 5 min at 0°C. 2-aminomethylpiperidine (**6**; 2.11 g, 18.5 mmol) was added and the icebath was removed. After 24 h stirring the colourless solid DCU was filtered off on a porosity 3 glass frit and rinsed colourless with DCM. The yellow DCM phase was washed with sat. Na_2CO_3, then 0.5M phosphate buffer at pH>10, then dried with brine, Na_2SO_4, filtered and evaporated to yield a yellow crude oil (6.6 g). The oil was left at 4°C overnight, and the remaining DCU crystallised and was filtered off as previously. NMR of this crude then indicated a mixture of **7** with N-acylurea byproduct **S1**. Column chromatography (1:1:0 → 1:1:1 EA:Cy:MeOH gradient) gave **7** (2.703 g, 42 %) as a colourless, crystalline solid.

Compound **7** has $R_f = 0.0$ in 1:1 Cy:EA, $R_f = 0.20$ in 4:4:1 Cy:EA:MeOH, and is stained by $KMnO_4$ as well as ninhydrin (pink charring purple). HRMS (TOF MS ESI$^+$) calcd for $[C_{17}H_{34}N_3O_3]^+ = [MH^+]$: *m/z* 328.2595, found 328.2589. The NMR spectra of **7** suggest the presence of two rotameric forms in approximate ratio 2:1, for each of the two diastereoisomers. HSQC, COSY and jmod spectra support the spectral assignment. ^{1}H- and ^{13}C-NMR spectra are given in the NMR Appendix. ^{1}H-NMR (200 MHz, $CDCl_3$): δ = 7.09-6.81 ((s, br + s, br), 1H, NH_{amide}), 5.70-5.34 ((s, br) + (d, br, ^3J=7.6 Hz), 1H, $NH_{carbamate}$), 4.08-3.98 (m, 1H, H2), 3.31-3.15 (m, 1H, H6), 3.11-2.90 (m, 2H, H6' + H7), 2.70-2.44 (m, 2H, 2×H11), 2.14 (s, br, 1H, shift varies strongly between spectra, NH_{amine}), 1.76-1.41 (m, 6H, 2×H3 + H4 + H8 + H9 + H10), 1.33 (s, 9H, 9×H14), 1.32-1.00 (m, 3H, H8' + H9' + H10'), 0.88 + 0.87 (d, ^3J=2.1Hz + d, ^3J=2.4Hz; 6H; 6×H5) ppm. ^{13}C-NMR (50 MHz, $CDCl_3$): Diastereoisomer 1: δ= 173.0 (C1), 155.7 (C12), 79.6 (C13), 55.8 (C7), 53.2 (C2), 46.5 (C11), 45.1 (C6), 41.4 (C3), 30.1 (C8), 28.3 (3×C14), 26.3 (C10), 24.7 (C4), 24.2 (C9), 22.9 + 22.0 (2×C5). Diastereoisomer 2: δ= 173.1 (C1), 155.8 (C12), 79.6 (C13), 55.5 (C7), 53.2 (C2), 46.5 (C11), 45.1 (C6), 41.3 (C3), 30.2 (C8), 28.3 (3×C14), 26.2 (C10), 24.7 (C4), 24.2 (C9), 22.9 + 22.0 (2×C5) ppm.

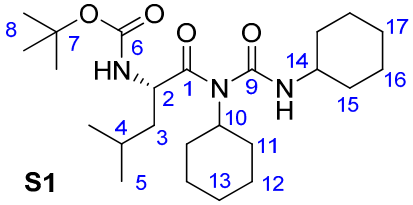

S1

S1 : 1-((*N*-*tert*-butoxycarbonyl)-L-leucyl)-1,3-dicyclohexylurea

Byproduct **S1** was isolated during syntheses of **7** and **9** as a colourless powder with $R_f = 0.91$ in 40:1 DCM:MeOH, stained by $KMnO_4$ as well as ninhydrin (pink charring orange). MS (ESI, positive mode): *m/z* 438,3: $[MH]^+$. HRMS (TOF MS ESI$^+$) calcd for $[C_{24}H_{43}N_3O_4Na]^+ = [MNa^+]$: *m/z* 460.3146, found 460.3125. The ^{1}H-NMR spectrum is given in the NMR Appendix. ^{1}H-NMR (200 MHz, $CDCl_3$): δ= 7.66 (d, br, ^3J=6.7 Hz, 0.9H, $NH_{carbamate}$), 4.92 (d, ^3J=7.0 Hz, 1H, H10), 4.39 (~q, $^3J\approx$7.1 Hz, 1H, H14), 4.12-4.10 (m, 1H, H2), 3.67-3.64 (m, 1H, NH_{urea}), 1.40 (s, 9H, 9×H8), 2.00-1.42 + 1.36-1.05 (m, 23H, H2 + 2×H3 + 4×H11 + 4×H12 + 2×H13 + 4×H15 + 4×H16 + 2×H17), 0.88 (d+d, ^3J=3.7 Hz + ^3J=3.8 Hz, 6H, 6×H5) ppm. ^{13}C-NMR (50 MHz, $CDCl_3$): δ= 172.1 (C1), 156.5 (C6), 153.6 (C9), 80.3 (C7), 54.8 (C10), 51.8 (C2), 50.1 (C14), 42.1 (C3), 33.5 + 32.6 (2×C15), 31.8 + 31.6 (2×C11), 29.3 (C3), 28.3 (3×C8), 26.1 + 26.0 (2×C16), 25.5 (C17), 25.4 (C13), 24.8 (C4), 24.6 (2×C12), 23.0 + 21.9 (2×C5) ppm.

8 : N^2-2-dimethylpropane-1,2-diamine
The title compound was synthesised in three steps adapted from literature procedures.

Acetone cyanohydrin: Following a procedure adapted from Faghihi *et al.*[S3], acetone (5.8 g, 100 mmol) was added to a stirred aqueous solution of sodium metabisulfite (11 g, 58 mmol, 20 mL). The subsequent addition of an aqueous solution of KCN (6 g, 92 mmol, 20 mL) resulted in the separation of the title compound in an upper phase. Upon completion of the reaction, the phases were separated and the upper phase was dried on Na_2SO_4 and filtered to give the title compound as a clear liquid (5.402 g, 69 %). MS (ESI, positive mode): m/z = 86.1: $[MH]^+$. ^{1}H-NMR (200 MHz, $CDCl_3$): δ = 1.43 (s, 6H, 2×CH_3) ppm. ^{13}C-NMR (50 MHz, $CDCl_3$): δ = 123.0 (C≡N), 65.3 (C(Me)$_2$), 29.4 (2×CH_3) ppm.

2-methylamino-2-methyl-propionitrile: Following a procedure adapted from Exner *et al.*[S4], to a 40 wt% aqueous solution of methylamine (2.8 g, 36 mmol) cooled in an icebath was slowly added acetone cyanohydrin (1 g, 12 mmol) such that the internal temperature did not exceed 15°C. After the addition was finished, the reaction mixture was stirred for a further 90 min, then extracted with Et_2O (3×10 mL). The combined organic phases were dried on Na_2SO_4, filtered, and concentrated under reduced pressure to give the title compound as a colourless liquid (0.700 g, 59 %). MS (ESI, positive mode): m/z = 99.1: $[MH]^+$. ^{1}H-NMR (200 MHz, $CDCl_3$): δ = 2.27 (s, 3H, NCH_3), 1.21 (s, 6H, 2×CH_3) ppm. ^{13}C-NMR (50 MHz, $CDCl_3$): δ = 122.8 (C≡N), 52.5 (C(Me)$_2$), 31.8 ($NHCH_3$), 27.5 (2×CH_3) ppm.

N^2-2-dimethylpropane-1,2-diamine (8):[S5] Following a procedure adapted from Chong *et al.*[S5], 2-methylamino-2-methyl-propionitrile (1.960 g, 20 mmol) was added dropwise to a suspension of $LiAlH_4$ (1.520 g, 40 mmol) in Et_2O (2 mL) under argon. The reaction was stirred for 3 hours at RT, diluted with Et_2O (30 mL) and cooled in an icebath. Sat. K_2CO_3 was added dropwise until evolution of hydrogen ceased. Solid Na_2SO_4 was then added to the reaction mixture which was stirred for 10 min before the salts were filtered off on Celite and washed with large quantities of Et_2O. The filtrate was concentrated under reduced pressure to give **8** as a clear, somewhat volatile liquid (2.001 g, 98 %) that may be more conveniently stored, cold, as a solution in Et_2O. MS (ESI, positive mode): m/z = 103.1: $[MH]^+$. ^{1}H-NMR (200 MHz, $CDCl_3$): δ = 2.40 (s, 2H, CH_2), 2.14 (s, 3H, NHC$\underline{H}_3$), 1.80 (s, br, 3H, NH + NH_2), 0.87 (s, 6H, 2×CH_3) ppm. ^{13}C-NMR (50 MHz, $CDCl_3$): δ = 53.0 (C(Me)$_2$), 50.2 (CH_2), 28.3 ($NHCH_3$), 23.0 (2×CH_3) ppm.

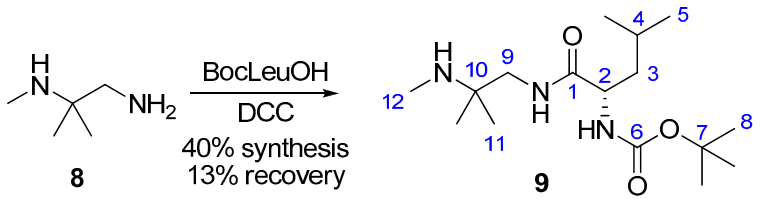

9 : (*N'-tert*-butoxycarbonyl)-L-leucyl-(2-methyl-2-(methylamino)propyl)amide

BocLeuOH (1.37 g, 5.92 mmol) in dry DCM (50 mL) at -5°C was reacted with DCC (1.23 g, 5.95 mmol, 1 eq) for 5 min, then 2-methylamino-2,2-dimethyl)aminoethane **8** (1.50 g of *ca*. 47 wt% solution in diethyl ether, *ca*. 6.9 mmol, >1 eq) was injected and the reaction left stirring at RT for 16h. After removing DCU by filtration, the amines were then extracted with aqueous HCl (2M, 3×30 mL); evaporation of the organic phase gave only N-acylurea byproduct **S1** (1.60 g, 3.65 mmol). The clear, acidic, combined aqueous phases were then basified with KOH to pH>12 and extracted with DCM (6×20 mL), and the new combined organic phases were dried on Na_2SO_4, filtered, and evaporated under reduced pressure to yield a colourless crude oil (0.54 g). NMR indicated a mixture of only two products: **9** (43 mol%, 52 wt%, 280 mg, 0.88 mmol) and a byproduct due to the loss of the Boc group (**S2**, 260 mg, 1.2 mmol). This mixture was filtered through a short silica column using a gradient of EA:Cy:MeOH (10:7:0→10:7:3) with which **S2** was immobile, and **9** was obtained as a colourless oil which solidified on standing (235 mg, 0.74 mmol, 13 %).

Compound **9** has $R_f = 0.10$ in 14:6:7 EA:Cy:MeOH and is stained by $KMnO_4$ as well as ninhydrin (purple charring black). HRMS (TOF MS ESI$^+$) calcd for $[C_{16}H_{34}N_3O_3]^+ = [MH^+]$: *m/z* 316.2595, found 316.2599. HSQC, COSY and jmod spectra support the spectral assignment. The raw ^{1}H-NMR spectrum is given in the NMR Appendix. ^{1}H-NMR (500 MHz, $CDCl_3$): $\delta = 6.80$ (s, br, 1H, NH_{amide}), 5.04 (~d, br, $^3J \approx 7.7$ Hz, 0.8H, $NH_{carbamate}$), 4.12-4.08 (m, 1H, H2), 3.26 (dd, $^2J = 14.0$ Hz & $^3J = 5.9$ Hz, 1H, H9), 3.17 (dd, $^2J = 13.3$ Hz & $^3J = 4.9$ Hz, 1H, H9'), 2.34 (s, 3H, 3×H12), 2.14 (s, br, 1H, NH_{amine}), 1.72-1.65 (m, 2H, H4 + H3), 1.54-1.49 (m, 1H, H3'), 1.46 (s, 9H, 9×H8), 1.11 (s, 6H, 6×H11), 0.96 (d, 3H, $^3J = 3.7$ Hz, 3×H5), 0.95 (d, 3H, $^3J = 3.6$ Hz, 3×H5') ppm. ^{13}C-NMR (125 MHz, $CDCl_3$): $\delta = 172.9$ (C1), 155.8 (C6), 80.0 (C7), 53.7 (C10), 53.5 (C2), 46.6 (C9), 41.4 (C3), 28.4 (3×C8), 28.3 (C12), 24.9 (C4), 24.6 (2×C11), 23.0 + 22.2 (2×C5) ppm.

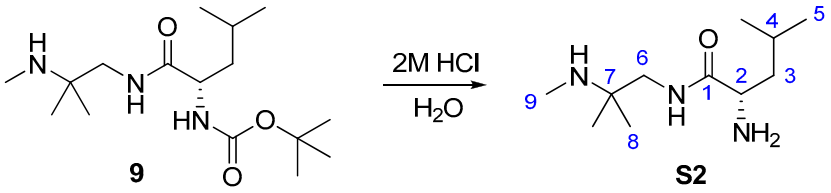

S2 : L-leucyl-(2-methyl-2-(methylamino)propyl)amide

This compound could be completely identified in the NMR spectra of crude **9**, but was not isolated after chromatography. The compound has R_f = 0.0 in 14:6:7 EA:Cy:MeOH and is stained by $KMnO_4$ as well as ninhydrin (red charring purple). HSQC, COSY and jmod spectra support the spectral assignment. ^{1}H-NMR (500 MHz, $CDCl_3$): δ = 7.43 (s, br, 0.9H, NH_{amide}), 3.27 (dd, ^3J=9.5 Hz & ^3J=4.3 Hz, 1H, H2), 3.02 (s, 2H, 2×H6), 2.17 (s, 3H, 3×H9), 1.62-1.50 (m, 2H, H3 + H4), 1.29-1.20 (m, 1H, H3'), 0.92 (s, 6H, 6×H8), 0.82 (d, ^3J=6.4Hz, 3H, 3×H5), 0.80 (d, ^3J=6.4Hz, 3H, 3×H5') ppm. ^{13}C-NMR (125 MHz, $CDCl_3$): δ = 175.9 (C1), 53.3 (C7), 52.7 (C2), 46.4 (C6), 44.3 (C3), 28.6 (C9), 24.8 (C4), 24.7 (2×C8), 23.4 + 21.4 (2×C5) ppm.

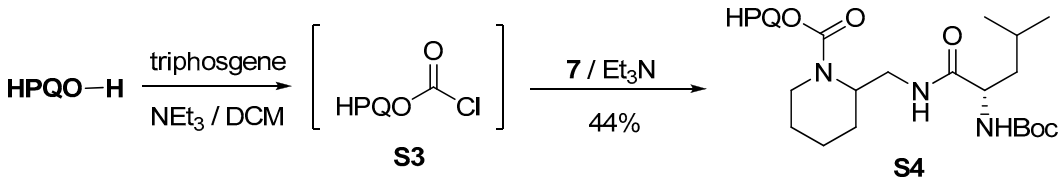

S4 : 2-(4-oxo-3,4-dihydroquinazolin-2-yl)phenyl 2-((*N'-tert*-butoxycarbonyl)-L-leucylamido)methyl)piperidine-1-carboxylate

Caution : phosgene, b.p. 8°C, is highly toxic and corrosive and reacts violently with many nucleophiles. Excess phosgene (formed by the amine-mediated decomposition of triphosgene) was caught in the primary liquid nitrogen trap and destroyed when still cold in DCM solution by its dropwise addition to a vigorously stirred, cold mixture of 2-aminoethanol or piperidine (5 mL) and ethanol (30 mL) in dichloromethane (100 mL) in a well-ventilated hood.

To **HPQO-H** (76 mg, 0.32 mmol) in a two-neck flask under argon was added CaH_2-distilled triethylamine stored on KOH (57 mg, 0.56 mmol, 2 eq), then dry DCM (1.2 mL), and the mixture cooled in an icebath. A solution of triphosgene (124 mg, 0.42 mmol) in dry DCM (1.2 mL) was injected with vigorous stirring, and the orange solution was stirred for 40 min at 0°C, then 20 min at 25°C, before all volatile components were removed at high vacuum with double liquid nitrogen traps to leave a beige solid containing **S3** (not isolated). A solution of amine **7** (19 mg, 0.058 mmol) and CaH_2-distilled triethylamine stored on KOH (101 mg, 1.00 mmol, 16 eq) in dry

DCM (8 mL) was injected at RT, forming an olive liquid which was stirred for two hours before being quenched by pouring onto sat. $NaHCO_3$. The aqueous phase was extracted with $CHCl_3$ and the combined organic layers washed with sat. $NaHCO_3$, water, brine, dried on Na_2SO_4, filtered and evaporated. The crude residue was taken into $CHCl_3$ and filtered on Celite to remove part of the residual **HPQO-H**; the filtrate was separated by column chromatography (EA:Cy:MeOH gradient 2:2:0 → 2:2:1) to yield **S4** as a colourless solid (15 mg, 0.025 mmol, 44 %).

Compound **S4** has R_f = 0.21 in 1:1 EA:Cy, R_f = 0.73 in 2:2:1 EA:Cy:MeOH, and is stained by $KMnO_4$ and ninhydrin (orange charring pink). HRMS (TOF MS ESI$^+$) calcd for $[C_{32}H_{42}N_5O_6]^+ = [MH^+]$: *m/z* 592.3130, found 592.3123. The NMR spectra of **S4** suggest the presence of two rotameric forms in approximate ratio 7:3, for each of the two diastereoisomers, giving up to four resonances per nucleus. The COSY spectrum supports the spectral assignment. The ^{1}H- and ^{13}C-NMR spectra are given in the NMR Appendix.

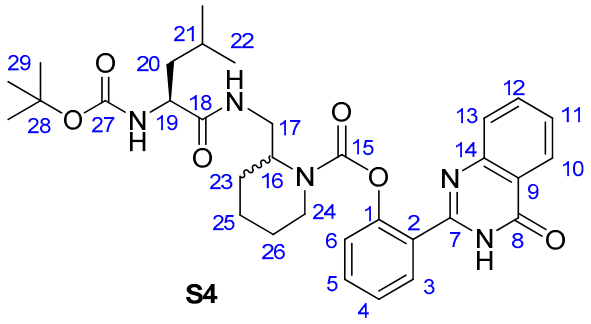

S4

^{1}H-NMR (500 MHz, $CDCl_3$): δ = 8.60 (s, br, 0.5H, 0.5×NH_{amide}), 8.36-8.11 (m, 2H, H10 + H3), 7.89-7.78 (m, 2.5H, H11 + H12 + 0.5×NH_{amide}), 7.58-7.47 (m, 2H, H5 + H13), 7.39-7.35 (m, 1H, H4), 7.31-7.15 (m, 1H, H6), 6.84 (s, br, 0.1H, 0.1×NH), 5.64 (s, br, 0.1H, 0.1×NH), 5.05-4.88 (d, br, ^3J=8.5 Hz + d, br, ^3J=6.5 Hz; 0.9H, $NH_{carbamate}$), 4.71-4.66 (m, 1H, H16), 4.46-4.34 (m, 1H, H19), 4.10-3.94 (m, 1H, H17), 3.87-3.51 (m, 1H, H17'), 3.43-2.89 (m, 2H, 2×H24), 1.77-1.45 (m, 9H, 2×H20 + H21 + 2×H23 + 2×H25 + 2×H26), 1.09-0.84 (m, 15H, 6×H22 + 9×H29) ppm.
^{13}C-NMR (125 MHz, $CDCl_3$): δ = 174.6 + 174.0 (C18), 163.4 + 162.9 (C8), 156.1 + 155.7 (C27), 153.5 + 152.8 (C15), 151.5 + 151.2 (C7), 149.9 + 149.7 (C14), 149.6 + 149.4 (C1), 134.9 + 134.8 (C12), 132.1 + 131.9 (C5), 131.0 + 130.7 + 129.8 (C3), 128.3 + 128.0 (C11), 127.3 + 127.1 (C9), 126.8 + 126.6 (C13), 126.6 + 126.1 (C4), 126.3 + 126.1 (C10), 124.6 + 123.1 (C6), 121.1 + 120.9 (C2), 79.8 (C28), 54.4 + 52.6 (C16), 53.1 + 50.8 (C19), 43.6 + 41.6 (C20), 41.3 + 41.2 + 39.7 (C24), 39.9 + 39.8 + 38.8 (C17) , 29.4 + 27.1 + 26.9 (C23), 28.3 + 28.2 + 28.0 (3×C29), 25.6 + 25.3 (C26), 24.9 + 24.9 (C21), 23.0 + 22.3 (2×C22), 19.6 + 19.3 (C25) ppm.

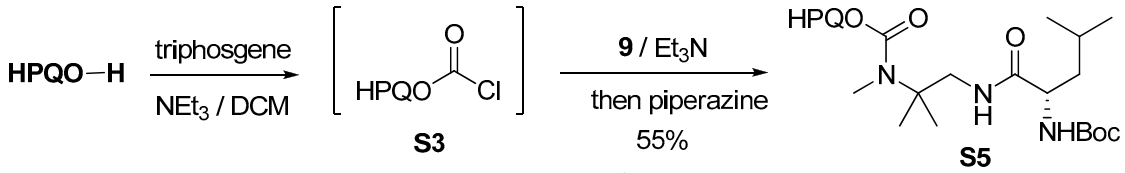

S5 : 2-(4-oxo-3,4-dihydroquinazolin-2-yl)phenyl N^1-((*N*-*tert*-butoxycarbonyl)-L-leucyl)-N^2-2-dimethyl-propane-1,2-diamino-N^2-carboxylate

S5 was synthesised from **9** (198 mg, 0.627 mmol) and **HPQO-H** (149 mg, 0.628 mmol) by the same method as for **S4**, but quenching excess **S3** with piperazine in dry pyridine before pouring onto $NaHCO_3$. Part of the crude yellow oil (200 mg of 299 mg) was taken into DCM (2×1 mL) and the soluble portion decanted then chromatographed (Cy:EA 3:1 → 1:1) giving **S5** as a dense colourless powder (134 mg, 0.231 mmol, i.e. 55 % yield overall), fluorescing weakly blue under 365 nm UV light. Compound **S5** has R_f = 0.22 in 1:1 EA:Cy, R_f = 0.61 in 10:10:1 EA:Cy:MeOH and is stained by $KMnO_4$ as well as ninhydrin (pink charring orange). HRMS (TOF MS ESI^+) calcd for $[C_{31}H_{42}N_5O_6]^+ = [MH^+]$: *m/z* 580.3130, found 580.3106. The NMR spectra of **S5** suggest the presence of two rotameric forms in approximate ratio 4:1. HSQC and COSY spectra support the spectral assignment. The ^{1}H- and ^{13}C-NMR spectra are given in the NMR Appendix.

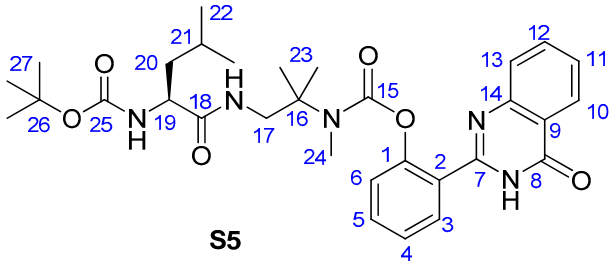

^{1}H-NMR (500 MHz, $CDCl_3$): δ = 8.29 (d, 7.8 Hz, 1H, H10), 7.91 (d, 7.3 Hz, 1H, 0.8×H3),7.79 (d, 2.2H, H12 + H5 + 0.2×H3), 7.55-7.48 (m, 2H, H11 + H13), 7.39-7.35 (m, 1H, H4), 7.24 (d, 8.3 Hz, 1H, H6), 6.84 (s, br, 0.8H, NH_{amide}),6.18 (s, br, 0.1H, NH_{amide}), 5.60 (d, br, ^3J=6.8 Hz, 0.7H, $NH_{carbamate}$), 4.23-4.03 (m, 1H, H19), 3.81-3.37 (m, 2H, 2×H17), 3.05 (s, 3H, 3×H24), 1.80-1.49 (m, 3H, H21 + 2×H20), 1.34 (s, 6H, 6×H23), 1.23 (s, 9H, 9×H27), 0.95 (d, ^3J=6.6 Hz, 3H, 3×H22), 0.93 (d, ^3J=6.5 Hz, 3H, 3×H22') ppm. ^{13}C-NMR (125 MHz, $CDCl_3$): δ = 173.8 (C18), 162.5 (C8), 155.8 (C25), 154.8 (C15), 150.7 (C7), 149.4 (C14), 149.2 (C1), 134.9 (C12), 132.3 (C5), 130.7 (C3), 127.9 (C11), 127.6 (C9), 127.2 (C13), 126.6 (C10), 126.4 (C4), 123.8 (C6), 121.1 (C2), 79.5 (C26), 60.9 (C16), 53.6 (C19), 46.5 (C17), 41.2 (C20), 32.7 (C24), 28.3 (3×C27), 25.3 (C21), 25.0 + 24.9 (2×C23), 23.2 + 22.0 (2×C22) ppm.

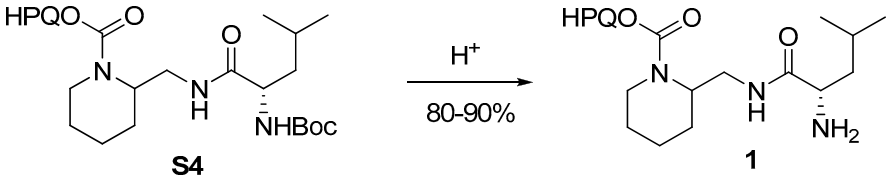

S4 **1**

1 : 2-(4-oxo-3,4-dihydroquinazolin-2-yl)phenyl 2-((L-leucylamido)methyl)piperidine-1-carboxylate

To **S4** (174 mg, 0.294 mmol) were added *p*-TsOH.H_2O (61 mg, 0.318 mmol) and dry EtOH (10 mL), and the solution stirred at 80°C under a closed argon atmosphere for 8 h. TLC on 1:1:1 EA:Cy:MeOH, revealing with 254 and 365 nm UV and ninhydrin, was used to monitor reaction progress. After concentration under reduced pressure, column chromatography using eluants of EA:Cy:MeOH was used to purify the tosylate salt of **1** before enzymatic testing, eluting residual **HPQO-H** with 1:1:0, unreacted **S4** with 1:1:0.15, and crude tosylate of **1** with 1:1:1 (149 mg, containing a slight excess of *p*-TsOH, 80 %) as a colourless powder fluorescing blue under 365 nm UV light. Trituration of the crude tosylate of **1** with water (1.5 mL per 100 mg) removes excess *p*-TsOH without dissolving much **1**, leaving the pure tosylate salt of **1** as determined by NMR, as a colourless powder. Methanol can be used to dissolve the tosylate salt (~0.5 mL per 100 mg) before its dilution into water, without reprecipitation.

Alternatively, the TFA salt of **1** could be prepared in 80-90 % yield following a similar protocol as given for **2**. HRMS (TOF MS ESI$^+$) calcd for $[C_{27}H_{34}N_5O_4]^+ = [MH^+]$: *m/z* 492.2606, found 492.2588. The TFA salt of **1** has $R_f = 0.20$ in 2:2:1 EA:Cy:MeOH, and is stained by $KMnO_4$ as well as ninhydrin (vivid orange). The TFA salt of **1** was easily soluble in D_2O and with a suitable acquisition time (4 s / scan) good NMR spectra were obtained. The 2 diastereoisomers each appear to have an approximately 2:1 ratio of rotamers in this solvent. HSQC and COSY spectra support the spectral assignment. The ^{1}H- and ^{13}C-NMR spectra are given in the NMR Appendix.

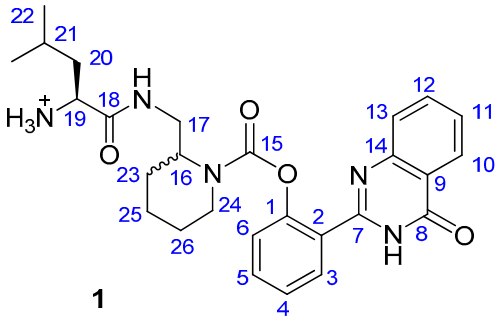

1

^{1}H-NMR (D_2O, TFA counterion, 500 MHz): δ = 8.20 (d, ^{3}J=8.1 Hz, 1H, H10), 7.94 (~t, ^{3}J≈7.9 Hz; 1H, H12), 7.77-7.70 (m, 3H, H3 + H5 + H13), 7.67 (~t, ^{3}J≈7.5 Hz, 1H, H11), 7.48 (~t, ^{3}J≈7.4 Hz, 1H, H4), 7.36-7.32 (d+d, each ^{3}J=7.9 Hz; 1H, H6), 4.56-2.73 (m, 6H, H16 + 2×H17 + H19 + 2×H24), 1.66-1.55 (m, 1H, 1×H26), 1.55-1.34 + 1.08-1.00 (m+m, 8H, 2×H20 + H21 + 2×H23 + 2×H25 + H26'), 0.80-0.70 (m, 6×H22) ppm. ^{13}C-NMR (D_2O, TFA counterion, 125 MHz): δ = 170.5 + 170.3 (C18), 163.0 (q, ^{3}J(C,F)=35 Hz, TFA), 162.3 + 162.2 (C8), 154.1 (C15), 153.9 + 153.8 (C7), 148.4 + 148.2 + 148.1 (C14), 141.7 + 141.3 (C1), 137.1 + 137.1 (C12), 135.1 + 134.8 (C5), 130.2 + 130.2 (C3), 129.6 (C11), 127.0 (C10 + C4), 123.6 + 123.4 + 123.3 (C6), 122.4 + 122.3 (C9), 122.1 + 122.0 + 121.9 (C13), 119.2 (C2), 116.4 (q, ^{2}J(C,F)=294 Hz, TFA), 52.0 + 51.9 + 51.8 (C16), 51.6 + 51.5 + 51.4 + 50.9 (C19), 40.5 + 40.1 (C24), 40.0 + 39.9 (C20), 38.2 (C17), 25.8 + 25.6 (C23), 25.0 + 25.0 + 24.5 (C26), 23.9 + 23.9 + 23.8 (C21), 21.8 + 20.9 + 20.9 (2×C22), 18.1 + 18.0 (C25) ppm.

The ^{1}H- and ^{13}C-NMR spectra of the tosylate salt of **1** (in CD_3OD) were similar to that of its TFA salt (in D_2O), but without the peaks for the TFA anion in the ^{13}C-NMR spectrum, and with the following peaks for the tosylate counterion: ^{1}H-NMR (CD_3OD, tosylate counterion, 500 MHz): δ = 7.73 (d, ^{3}J=8.0 Hz, 2H), 7.26 (d, ^{3}J=7.8 Hz, 2H), 2.39 (s, 3H) ppm; ^{13}C-NMR (CD_3OD, tosylate counterion, 125 MHz): δ = 142.0, 140.6, 128.6 (×2), 126.0, 125.7 (×2).

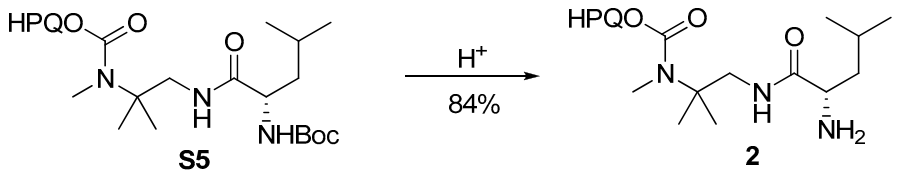

S5 **2**

2 : 2-(4-oxo-3,4-dihydroquinazolin-2-yl)phenyl N^1-L-leucyl-N^2-2-dimethyl-propane-1,2-diamino-N^2-carboxylate

To **S5** (56 mg, 0.097 mmol) was added dry DCM (1.5 mL) and TFA (1.5 mL). The reaction was stirred under argon at RT for 1 h, then high vacuum was gradually applied leaving a colourless

powder (the TFA salt of **2**, yield > 90 %). TLC of the crude revealed neither **HPQO-H** nor **S5**, but it was submitted to column chromatography using a gradient of EA:Cy:MeOH (1:1:0→1:1:1) before enzymatic testing, giving the TFA salt of **2** (48 mg, 0.081 mmol, 84 %) as a dense colourless powder fluorescing faintly blue under 365 nm UV light. HRMS (TOF MS ESI$^+$) calcd for $[C_{26}H_{34}N_5O_4]^+ = [MH^+]$: *m/z* 480.2606, found 480.2594. The TFA salt of **2** has $R_f = 0.0$ in 1:1:0 EA:Cy:MeOH, $R_f = 0.76$ in 1:1:2 EA:Cy:MeOH, and is stained by ninhydrin (vivid red). The udeft ^{13}C-NMR sequence[S6] proved necessary to observe the five quaternary carbon peaks marked with an asterisk (*). HSQC, HMBC and COSY spectra support the spectral assignment. The ^{1}H- and ^{13}C-NMR spectra are given in the NMR Appendix.

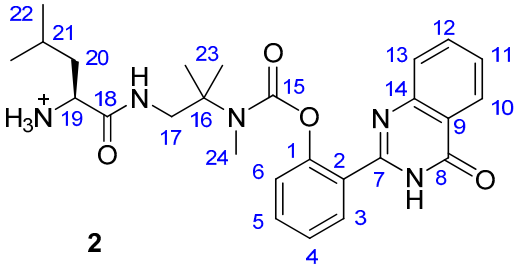

2

^{1}H (D_2O, TFA counterion, 500 MHz): $\delta = 8.02$ (d, ^3J=8.2 Hz, 1H, H10), 7.81-7.77 (m, 1H, H12), 7.64 (dd, ^3J=7.4 Hz & ^3J=1.7 Hz, H3), 7.60-7.56 (m, 2H, H5 + H13), 7.50-7.47 (m, 1H, H11), 7.40-7.37 (m, 1H, H4), 7.24 (d, 8.2 Hz, 1H, H6), 3.81 (t, ^3J=7.4 Hz, 1H, H19), 3.41 (d, br, ^3J=13.4 Hz, 1H, H17), 3.08-3.00 (m, 1H, H17'), 2.93 (s, 3H, 3×H24), 1.54-1.41 (m, 3H, 2×H20 + H21), 1.02-0.83 (s, br + s, br, 6H, 6×H23), 0.82 + 0.80 (each d, ^3J=4.6 Hz; 6H, 6×H22) ppm. ^{13}C-NMR (D_2O, TFA counterion, 125 MHz): $\delta = 170.4$ (C18), 164.4 (*C8), 163.0 (q, ^3J(C,F)=35 Hz, TFA),154.5 (*C15), 151.6 (*C14), 148.3 (C1), 147.8 (*C7), 136.0 (C12), 132.9 (C5), 129.7 (C3), 128.1 (C11), 126.5 (C10), 126.2 (C13), 126.0 (*C9), 126.0 (C4), 123.3 (C6), 119.7 (C2), 116.4 (q, ^2J(C,F)=294 Hz, TFA), 59.4 (C16), 52.0 (C19), 45.9 (C17), 40.0 (C20), 32.1 (C24), 24.0 (C21), 23.8 (2×C23), 21.6 + 21.2 (2×C22) ppm.

Enzymatic Testing

Preamble

Probes **1** and **2** do not display any ESIPT fluorescence as their phenol is carbamylated, so no excited-state phenol-to-imine hydrogen transfer is possible. As it is the ESIPT mechanism that is responsible for very large Stokes shift (>130 nm) in the fluorescence spectrum of **5**, when probes **1** and **2** are not activated, they give almost no background fluorescence signal under appropriate measurement conditions (see Fig. 2a and **Experimental Design**). The enzymatic cleavage of the terminal leucine residue of the probes exposes the amine termini of their spacers in species **S6** and **S7**; these then cyclise spontaneously to generate ureas (**3** and **4**), releasing the ESIPT fluorophore **5** (Scheme S1). Once the solubility limit for **5** has been surpassed and nucleation has commenced, the precipitating **5** (HPQO-H) gives a strong ESIPT fluorescence signal.

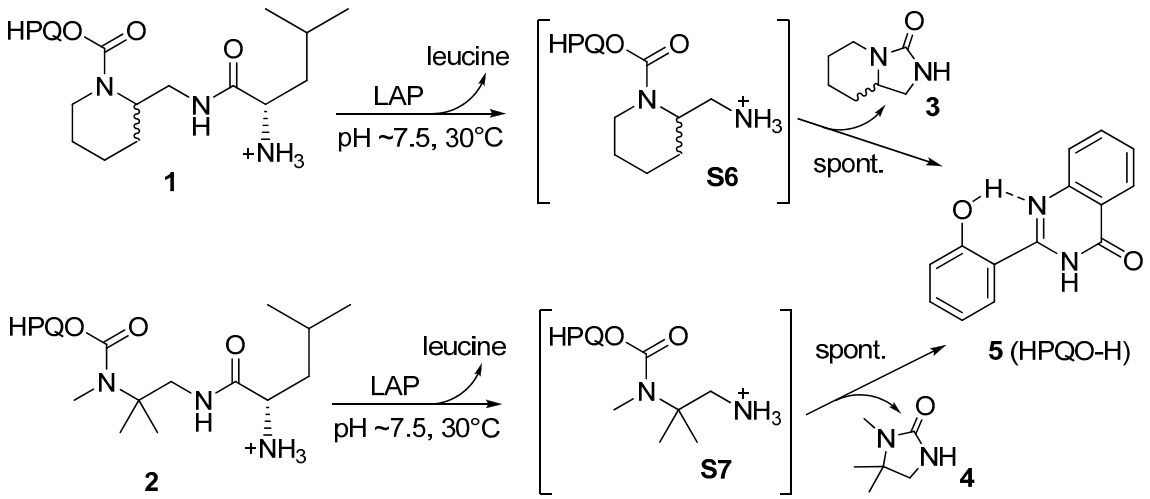

Scheme S1 Enzymatic cleavage of the aminopeptidase-targeting substrates of probes **1** and **2** results in fast, spontaneous cyclisation of their spacers and liberation of the fluorophore **5**.

Typical Enzymatic Tests: Visual Results (Photographs and Scanning Test Image)

A sequence of photographs taken with a standard personal digital camera (Canon IXUS 110) of the activation of probe **1** by leucine aminopeptidase (LAP) enzyme in pH~7.5 buffer at RT is shown in Fig. S1. The top left panel is a bright-field image, all other images are obtained from visible-spectrum fluorescence under 365 nm irradiation. The evolution of the fluorescence signal with enzyme activation can be seen (vials **2**† and **3**†), as well as the absence of spontaneous signal generation (other vials). Vials **2**† and **3**† contain probe **1** at ~100 μM, with LAP at ~1/50 of its concentration in the kinetic experiments; the other vials are controls lacking either enzyme or substrate.

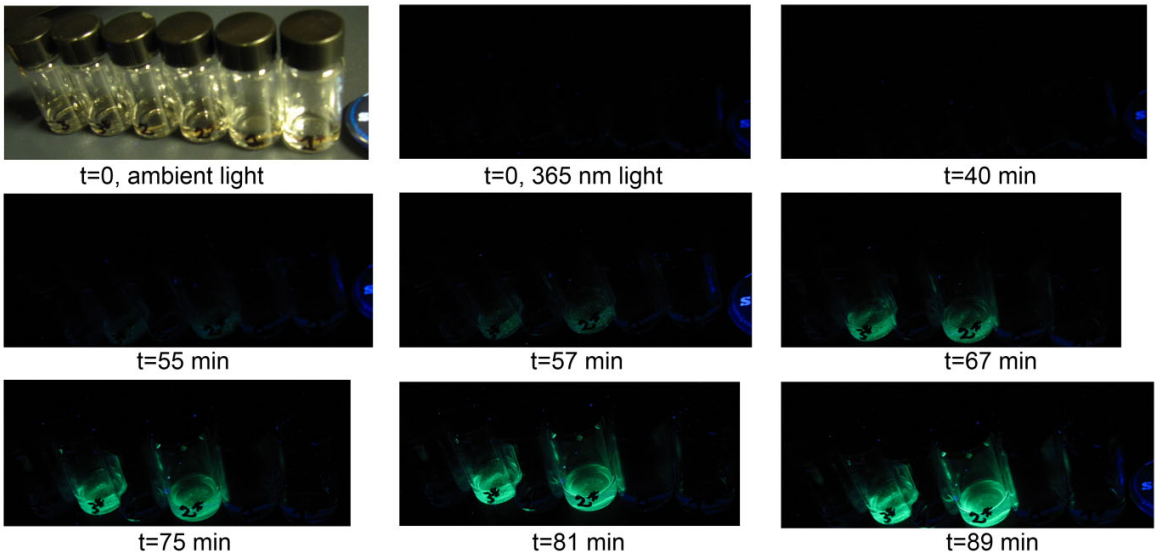

Fig. S1 Enzymatic activation of probe **1** by LAP. A fluorescence signal appears over time when the probe is activated by LAP (vials **2**† and **3**†), but zero fluorescence signal is seen in the absence of enzymatic activation (other vials). A blue-fluorescent marker is occasionally visible at the right of the wider images and gives a rough indication of a constant level of fluorescence for normalisation of the images' intensities. A detail of this image was presented as Fig. 1 in the main article, with simple +15% enhancement of both brightness and contrast for better printability (implemented with the Paint.NET program); no brightness/contrast enhancements are present in this image.

Fig. S2 shows a photograph taken with the same camera and similar settings, of a vial containing a pH~7.5 buffered solution of probe **1** concentrated to 2000 μM. The vial was left standing at RT; only after three weeks could some tiny fluorescent crystals be seen under 365 nm irradiation, indicating some spontaneous hydrolysis over this timescale. The image may however be compared to the images in Fig. S1 (for 100 μM initial concentration of probe **1**, enzymatically activated at low enzyme loading, after <1.5 h), to give an impression of the low absolute signal this represents, as well as the very much longer time needed for its appearance.

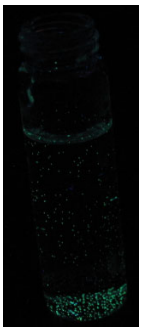

Fig. S2 After three weeks' standing at RT when concentrated to 2000 μM, probe **1** showed the precipitation of some tiny crystals of **5**, giving an indication of the timescale needed, even at this high concentration, for spontaneous hydrolysis to be detectable.

Fig. S3 shows a detail of a greyscale fluorescence image (darker=more fluorescence) of a microplate from a typical scanning-mode test (see **Experimental Design**) of compound **1** (image taken after 40 h incubation). The three series of active wells (containing a variable concentration of probe **1**, with a fixed concentration of LAP enzyme) illustrate the relationship between the observed signal and the initial concentration of **1**: wells with 209 μM (B2, D4, F6, H8) show more signal than those with 80 μM (B8, D2, F4, H6), or 21 μM (B6, D8, F2, H4). The other wells are controls, either containing distilled water for signal background measurement (B4), or no-enzyme controls (*i.e.* with probe **1** but without enzyme: H2 at 209 μM; D6 and F8 at 80 μM).

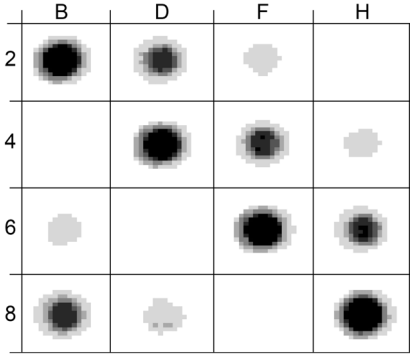

Fig. S3 Detail of a scanning mode fluorescence image of a microplate, taken after 40 h incubation. See text above for details.

The probe is robust (there is no false positive fluorescence signal arising from spontaneous hydrolysis of the carbamate linkage) and in its pro-fluorescent state is truly 'off' (the unactivated probe wells are indistinguishable from the no-substrate control even after 40 h). Note too the distribution of wells to combat evaporative effects and signal crosstalk (see **Experimental Design**).

Experimental Design

To validate the robustness of our off-ON probes as a practical, extensible system, we specifically desired to perform our tests in conditions which would be easy to apply to a range of peptidases present in near-physiological concentrations, without requiring highly optimised detection procedures, even if this were to imply a certain sacrifice of sensitivity. In the event, our probes performed outstandingly well (Fig. 2a), generating fluorescence signal-to-control ratios (measured after 11 h) above 1000:1, in conditions accessible to standard laboratories, without requiring vast quantities of enzyme to be used. By way of an example, while other current

phenolic probe research has required *e.g.* 5 U of enzyme per measurement[S7], our kinetic experiments typically used only 10 mU. Although enzymatic activity in Units as commercially advertised may not necessarily reflect the speed of enzymatic processing of a particular probe, the 500-fold difference between the enzyme activities used in such studies and our own can nevertheless be considered significant, and our experimental design therefore consciously risked giving slower signal generation than such high-loading studies. By way of an example, in the case cited above (using a phenolic glycoside),[S7] the experiment using 5 U enzyme (for 1 μM probe) was apparently complete after *ca.* 8 min. It should be noted that the no-enzyme control data given in that report (although under different conditions, with 10 μM probe, and not analysed in that publication) appeared to show a steady signal increase, presumably due to spontaneous probe hydrolysis, attaining over 5% of the signal seen for the corresponding active experiment – after only 30 min of incubation.[S7] Such instability would indeed force the choice of a short experimental timescale paired with a high enzyme loading to display acceptable probe performance; however this is far from the ideal case of true off-ON behaviour. By contrast, our probes were designed to feature immense stability towards spontaneous hydrolysis (Fig. 2b), to permit the use of these probes over far longer time scales, without needing to fear spontaneous signal generation reducing the signal-to-control ratio. Effectively, our probe tests could compensate for our comparatively sparing use of the model trigger enzyme by a longer period of its application. It was hoped that this measure would highlight the attractiveness of our probe system for the sensitive, no-background-signal imaging of more normal enzymatic activities (neither mutant strain cells nor other high-loading scenarios).

Fluorescence measurements were performed on a Mithras LB 940 microplate fluorimeter controlled by MikroWin software, using black 384-well microplates with 110 μL maximum well volume (Nunclone, NUNC Inc) for kinetic tests and black 96-well microplates with 220 μL maximum well volume (Corning, Corning Inc) for scanning tests. Tests were conducted at 29-30°C since a temperature of 37°C too rapidly resulted in the evaporation of the test solutions, and the use of an optical film to stop this evaporation lowered the sensitivity of the detection. The 4 mm beamwidth setting was chosen to cover the greatest area of each well (well width = 4 mm for the 384-well microplates, 9 mm for the 96-well microplates). To prevent any possible crosstalk of fluorescence signal from neighbouring wells, only wells lying on the intersection of

every second row and every second column were used, with the other wells being filled with water to try to slow evaporation. Wells around the rim of the microplate showed faster evaporation than those in the centre, so the column and row of wells on the border of the well plate were not used for testing and were filled with water. To combat other spatially-dependant evaporation effects, each series of wells was distributed across the microplate (see Fig. S3).

Excitation was performed at 355 nm and fluorescence was monitored at 510 nm (each selected with a 10 nm bandpass filter). Kinetic tests and scan-mode tests were designed to resemble two desired applications of this probe technology, namely high-throughput screening and cell counting, respectively. Kinetic tests delivered results in the form of a series of fluorescence signal readings (in RFU) per well per time point within a time range which could in practice extend to around 20 h, but was more reliable under 12 h due to constant evaporation of the well solutions; scanning mode tests delivered a fluorescence reading for each pixel in each well's acquisition grid and were conducted at specific time points (eg t=1 h, t=2 h, t=24 h etc.) during incubation. Kinetic measurements were performed with 3 seconds acquisition per data point and a lamp power setting of 10000 arbitrary units (calibrated to a software internal standard) as this gave satisfactory signal without saturating the detector; scanning measurements used 0.25 s acquisition per pixel and a lamp power setting of 30000 arbitrary units. The detection sensitivity of the fluorimeter itself was observed to vary during the initial 20-60 minutes of acquisitions then roughly stabilize, so dummy acquisitions were launched directly before the data acquisitions to permit better stabilisation of the lamp temperature, photomultiplier tube voltage, and other factors influencing detection stability. Kinetic test acquisitions were performed in the "Repeated" mode, with microplate shaking for 10 seconds between each plate acquisition, giving one acquisition point for all 77 wells used every 5.5 minutes. Scanning mode tests were performed in the "Scan" mode, typically with a 20×20 pixel acquisition grid set to completely cover the well of interest. Due to software requirements this actually implies setting the acquisition grid to cover also one well radius into the eight neighbouring wells, which in our experiments were filled with pure water to prevent false signal contributions (crosstalk); thus the true measurement grid lying directly over the well of interest is of approximately 10×10 pixels. Due to the 4 mm beamwidth, some pixels centred outside this real-signal area still show a fluorescence signal from pixel area overlap (as can be seen in Fig. S2). A typical acquisition duration for a single scan was therefore around 30 minutes for the 15 wells.

Enzymatic Testing Procedure

To partially simulate physiological media, all tests were conducted at pH~7.5, buffered with Tris/Tris.HCl (25 mM) and containing 12 mM NaCl. Stock solutions of the substrates were prepared fresh before each run by weighing precisely ~2 mg of the substrate salt, adding 0.2 mL MeOH to dissolve it, and diluting this stock with pH~7.5 buffer (with secondary dilutions when needed) such that the volume of substrate stock to be added to the well lay between 15-50 μL. In a typical run, such substrate stocks (from 70 – 400 μM) were left standing for approximately 2-3 hours at RT before the acquisition was launched, although the 378 μM data series for probe **1** presented in Fig. 2a was prepared from a solution that had been left standing for three weeks (illustrating a different practical aspect of the robustness of the probe system).

Microsomal neutral leucine aminopeptidase from porcine kidney (LAP, EC 3.4.11.1) was purchased from Sigma (Lot number 069K7356V) as a suspension in ammonium sulfate (3.5 M) containing $MgCl_2$ (10 mM), with 3.5 $mgmL^{-1}$ protein content and 10-40 U/mg protein reported for the standard substrate leucyl *p*-nitroanilide. LAP enzyme stock was prepared by diluting 10 μL of the enzyme suspension (stored at 4°C for less than 40 days before use) into 2 mL of the pH~7.5 buffer and shaking, then leaving at RT for at least 1 h, as incubation of the enzyme with $MgCl_2$ or $MnCl_2$ (as described elsewhere[S8]) was not observed to give an improvement of signal generation kinetics.

Water and/or pH~7.5 buffer were then added as needed to each well such that both the total volume and the buffer concentration were identical in all wells, irrespective of the volume of substrate stock to be added. The substrate stocks were then added. The final step was the addition of 20 μL of the enzyme stock to each of the active wells, so that in the kinetic tests the final concentration of enzyme was ~3.5 μgmL^{-1} (~60 nM[S9]), with approximately 10 mU of activity per well for the standard substrate leucyl *p*-nitroanilide, based on the activity quoted by the supplier. This addition was performed rapidly and in the same order in which the wells were to be read, giving approximately ± 2 minutes difference between the average real time elapsed after mixing and the fixed time as given by the microplate reader, to enable the best comparison of data between different wells. After the addition of the enzyme, the contents of each well were homogenised by triple aspiration and expulsion of the contents, and then the plate was loaded

into the fluorimeter and acquisition started. The time delay before the first acquisition (approximately 10-15 minutes) was factored in to the data during treatment.

Data Series and Treatment: Kinetic Tests

In each run, data were acquired from at least five replicates for each set of conditions used with enzyme-activated probes, or from at least three replicates for the controls (either no substrate or no enzyme). The parameters varied were substrate type, substrate concentration, and enzyme presence or absence. The raw data were obtained as series of fluorescence measurements in Random Fluorescence Units (RFU) over time. The raw data for each well are denoted $A_{X,I}(t')$, where X indicates the set of conditions in that well, I indicates the number of the replicate within the set of wells with those same conditions, and t' is the number of the data point in the acquisition series, *e.g.* t'=1 for the first data point acquired, t'=2 for the next, etc. The series $A_{X,I}(t')$ were first checked to confirm that no detector saturation had taken place. Then, three steps of data treatment were performed to give fluorescence signals $F_X(t)$ for each set of conditions X over real elapsed time *t*, with background signal subtraction, normalisation, outlier rejection and replicate selection performed as follows:

1) Firstly, a background signal (due to scattering from the plate and the solution and noise in the system) was subtracted, and data were normalised over time (to compensate for temporal drift in detector sensitivity or lamp luminosity, permitting a more reliable quantitative comparison of the data over the long acquisition times of the experiment). The data from wells containing only enzyme in buffer were averaged to give the background signal B(t'), and normalisation was performed by multiplication of the series by the factor B(1)/B(t'). Thus the signals $G_{X,I}(t')=[A_{X,I}(t')-B(t')]\times B(1)/B(t')$ were obtained.

2) Outlier data points were then discarded from each series if they were suitably different from their neighbours. It was considered that such outliers (*e.g.* points differing in intensity by up to a factor of 3 from the mean of the two neighbouring points) were not all necessarily due to true spikes in fluorescence signal, but that some were due to detection faults, *e.g.* the presence of strongly scattering dust particles in the beam path, which could justify their deletion. Arbitrarily, 5% of the data points from each series were deleted, as determined by the following algorithm:

For each series $G_{X,I}(t')$, a series of expected values $\mu_{X,I}(t')$ was calculated as per $\mu_{X,I}(t') = [(3G_{X,I}(t'-3) + 2G_{X,I}(t'-2) + 2G_{X,I}(t'+2) + 3G_{X,I}(t'+3))/10]$. Data points further from the point of interest were more heavily weighted than nearer data points to compensate for the observed effect that such outliers often occurred in spikes of two to three data points, possibly due to *e.g.* the temporary settlement of a dust particle on the plate near the well being read. A weighted mean-squared difference function $\Delta_{X,I}(t') =[G_{X,I}(t') -\mu_{X,I}(t')]^2/[| \mu_{X,I}(t')| + |G_{X,I}(t')|]$ was then calculated, and the points $G_{X,I}(t')$ giving the greatest values of $\Delta_{X,I}(t')$ deleted one by one, with recalculation of $\mu_{X,I}(t')$ and $\Delta_{X,I}(t')$ between every deletion. If the outlier data points thus rejected (approximately 5-10 per series) corresponded to the region where the fluorescence signal began to be noticeable, they were reinstated, since this algorithm was unsuited for application to regions with an inherently non-linear signal. Treatment of the first and last three data points in a series required unidirectional calculation of $\mu_{X,I}(t')$.

3) Data series $G_{X,I}(t')$ within each set X of replicates were then compared to see whether they were consistent; series inconsistent with the others in their set were discarded in the following way. The mean $M_X(t')$ of all series in a set was calculated, and then the average value $Q^*_{X,I}$ of the mean-squared error function $Q_{X,I}(t') =|[G_{X,I}(t') - M_X(t')]^2/M_X(t')|$. To reject a series I, the ratio $R_{X,I} = [Q^*_{X,I}$ / (the average value of the last five points of $M_X(t'))]$ had to be above an arbitrary threshold, chosen as 0.025. After having rejected the replicate with the largest $R_{X,I}$, the procedure was followed again (with prior recalculation of $M_X(t')$, $Q_{X,I}(t')$ and $R_{X,I}$) until either only three series remained in the set X, or until all series had $R_{X,I} \leq 0.025$. Then, data from corresponding time-values of these remaining replicates were averaged, and the dummy times t' converted to true elapsed times *t* since the addition of the enzyme, to give the fluorescence signals $F_X(t)$ as graphed and discussed in the main text.

Data Series, Treatment and Results: Scanning Tests

Only the data corresponding to pixels over the true well area, *i.e.* typically a central 10×10 pixel grid from an original 20×20 pixel grid, were retained. Due to overlap of the data contained in each pixel with their neighbouring pixels (typical settings : pixels nominally ~1×1 mm, but fluorimeter beamwidths ~4 mm), the data of these scan-mode tests were not considered necessarily quantitative in nature, although in the event, despite a simplistic treatment, they

proved to give final signals which linearly correlated to the original concentration with around 10% error. Rather than aiming for quantitative results though, their purpose was to give high sensitivity towards the detection of small amounts of signal *e.g.* for evaluating probe stability: the scan method ensured that the entire well was scanned (in case of situations such as *e.g.* where only one crystal of **5** may have formed, in a corner of the well not usually reached by the "Repeated" mode measurements) and that each true gridsquare was in effect scanned multiple times. Data acquired could be visualised as a linear-scaled greyscale plot of fluorescence reading *vs*. pixel location on the well (Fig. S2), where as shown earlier, the unactivated probe at concentrations up to 209 μM is indistinguishable after 40 h incubation from the no-enzyme controls based on these plots (both blank and control appearing entirely without any grey pixels next to the active wells). Numerical data treatment was as follows: RFU readings from the central 10×10 pixel grids were averaged to give a single RFU value per well per time point, and these values were filtered for consistency as per step 3) in the kinetic test data treatment section, discarding down to a minimum of two replicates per series to obtain $A_X(t)$ as a raw RFU value of wells near the mean in their set. These were then corrected by subtraction of the instantaneous background reading B(t) determined using the *pure-water-only* wells as a *minimum* estimate of background noise in the fluorescence acquisitions, and the resultant $G_X(t)$ were then either examined as a ratio over B(t) or multiplied by a factor with units μM / RFU intended to linearly correlate their fluorescence to their hydrolysed concentration (Table S1).

Table S1 Raw, background-subtracted, and multiplied signals from a scan-mode experiment. Brackets indicate that the data point was used to calibrate the values of the others in its column.

	$A_X(t)$ (RFU)		**$G_X(t)/B(t)$**		**Est Max Conc Hydrolysed (μM)**	
Well Series	**24 h**	**40 h**	**24 h**	**40 h**	**24 h**	**40 h**
Water	72839	73029	(0)	(0)	(0)	(0)
81 μM, NoEnz	78944	82526	0.08	0.13	0.26	0.40
209 μM, NoEnz	86302	94865	0.18	0.30	0.58	0.92
209 μM	4900858	5042099	66.3	68.0	(209)	(209)
81 μM	2415589	2462269	32.2	32.7	101	101
21 μM	511910	543580	6.03	6.44	19.0	19.8

Next, it was considered that the solubility threshold *S* of this particular ESIPT fluorophore **5** is nonzero, as can be seen by the consistent display of a lag time before signal generation in the kinetic experiments (see Fig. 2a), and in fact probably lies around 6 μM, based both on

examination of that data (see **Results: Kinetic Tests**), and data published for a similar fluorophore[S10]. Therefore assuming ~linear spontaneous hydrolysis kinetics when only a small fraction of the probe is hydrolyzed, we can expect that after a time *a*, the appearance of a fluorescence signal corresponding to an apparent hydrolysed concentration *x* μM indicates a true hydrolysed concentration of (*S*+*x*) μM. If a linear regime is obeyed, after a further time period *b*, we can therefore expect a fluorescence reading corresponding to an apparent concentration of ((1+*b*/*a*)(*S*+*x*)-*S*) μM. The increase of the $G_X(t)$ values for the no-enzyme control wells between the 24 h and 40 h readings would therefore predict a maximum solubility threshold *S* of **less** than 0 μM, assuming that these fluorescence signals arose from true spontaneous hydrolysis. (Note that the observed error in the calibration of hydrolysed concentration to fluorescence signal $G_X(t)$ for these scan mode measurements can be seen to be on the order of 10% (Table S1), which is insufficient to conclude that such a calculation cannot be applied to these wells). From this consideration alone, it can reasonably be concluded that the substrate hydrolysis in these 81 and 209 μM wells did not in fact reach the solubility threshold *S* during the first 24 hours of these high-sensitivity scan mode control experiments. This implies that the fact that the 24 h 'fluorescence readings' for the two controls were above the background, pure-water level is *not* due to spontaneous hydrolysis: that is, that the probe system at 200 μM is entirely stable within fluorescence-detectable limits over more than 24 h.

By similar logic, lacking further data points, no definite conclusions can be drawn about possible hydrolysis at the 40 h mark, and the reader is instead left to draw their own conclusions as to the general ease with which signal can be distinguished from background noise, and/or from possible spontaneous degradation, with reference to the raw scan-mode data (Table 1). Two supplementary points may be relevant. Firstly, the probe counterion of **1** used in these experiments was *p*-TsO^-; as discussed in the section **Results: Kinetic Tests**, it is possible that this ion contributed to the observed fluorescence signal of the controls. Secondly, over this time scale, evaporation – even though limited as much as possible between acquisitions – was a problem, and this could lead to partial deposition of the probe, with or without its counterion, or any other species from the solution onto the walls of the well, thus giving a falsely high background-subtracted fluorescence signal by scattering. Note however that this possible signal would still be less than 1/200 of that given by the fully activated probe, and that in the worst of cases (signal beginning to be noticeable immediately after the 24 h datapoint) spontaneous

hydrolysis would have begun to be detectable only after more than 140 times the detection delay for the activated probe (Fig. 2a).

Results: Kinetic Tests

The results of representative kinetic tests were presented in Fig.s 2a-2b and partially discussed in the main text. Note that the signals for probes **1** and **2**, at the same concentration, eventually reach the approximately the same fluorescence plateau values; this is expected if enzymatic hydrolysis is complete. While it is not clear that such a relationship should exist across all conditions for a solid-state fluorophore (where a Beer-Lambert type relationship cannot applied), we still observed a reasonable linear correlation between the plateau fluorescence values seen in the kinetic mode tests and the initial probe concentration (error <15%) calculated as follows. Plateau values were first obtained for signal-stabilised probe concentrations by averaging their signals between t=500 min and t=660 min. A 'true' concentration was defined as the known solution concentration of probe at t=0, and an 'effective' (signal-generating) concentration defined as the true concentration minus a nonzero solubility threshold S, as discussed in the section **Data Series, Treatment and Results: Scanning Tests** (*i.e.*, the true concentration ≡ effective concentration defined with S=0). The plateau signals were then best-fitted by linear relationships to the true and effective concentrations, and these two relationships used to recalculate Predicted Concentrations (at t=0) to enable easier comparison of the success of these two approaches (Table S2). The fits were optimised by minimizing an "average error", defined as the average ratio of (the difference between the predicted and true concentrations) to (the true concentration), across all signal series; for the effective concentration case, this yielded S=5.7 μM. Notice that this solubility estimate sits well with the earlier-mentioned literature report for a similar compound,[S10] and is also reasonable in being under 18 μM (the 18 μM series are seen to give a substantial signal, indicating that the fluorophore released in these experiments indeed began to precipitate). However, note that even if a Beer-Lambert type relationship can be applied, two main sources of error affect this analysis : 1) if the enzymatic reaction slowed towards the end as substrate became scarce (see also discussion in **Data Series, Treatment and Results: Scanning Tests**) the plateau values observed at finite time (t=11 hours) would be underestimates of the true plateau fluorescence values (*i.e.* the real solubility threshold would be lower than the

calculated value); 2) continuous evaporation from the wells concentrates the test solutions (*i.e.* the real solubility threshold would be higher than the calculated value).

Table S2 Best-fit linear correlations of plateau signal fluorescence with concentration, either assuming zero solubility, or simultaneously optimizing a solubility threshold (yielding *S*=5.7 μM). Plateau signal values are given as obtained from the software (not all the figures are significant).

Probe Series	Plateau Signal (RFU)	Predicted Conc., S=0 (μM)	Predicted Conc., S=5.7 (μM)
1, 378 μM	37517704	414	378
2, 100 μM	8661333	96	92
1, 100 μM	9711571	107	102
2, 59 μM	5631143	62	62
1, 59 μM	3861578	43	44
2, 32 μM	3749229	41	43
1, 32 μM	2351457	26	29
Average Error		***14.6%***	***11.9%***

Fig. 2a showed signals for both enzyme-activated and control experiments with probes **1** and **2** at 100 μM. Taking the crude ratio of the active to the control plateau signals (calculated as per the above method) yielded signal-to-control ratios of 630 (**1**) and 1485 (**2**) respectively, which average to approximately 1000:1. Fig. 2b presented, on a linear scale, the signal values for no-enzyme control experiments, showing that none of these controls gave any increase in signal over the 11 h of the experiment: thus if a *t*=0 fluorescence reading had been subtracted from their signals, the signal-to-control ratio would have been far higher still (2700 and 5000, for **1** and **2** respectively)! However, such a subtraction was expressly avoided during signal treatment, to illustrate that these probes may reliably be applied even where it may be impossible to simply 'subtract' *t*=0 readings to improve the observed sensitivity (for example, continuous diffusion of the unactivated probes into cells or tissues).

The three consecutive processes involved in signal generation are: 1) enzymatic hydrolysis of the amide bond in **1** or **2**; 2) spacer cyclisation releasing urea **3** or **4** and increasing the concentration of the solid-state fluorophore (**5**) in solution until its solubility limit (at 30°C, pH 7.5; it was estimated as per the above method as ~6 μM) has been surpassed and the solution becomes supersaturated; 3) subsequent nucleation and precipitation of **5**, thereby generating the observed fluorescence signal. Examining the signal traces (Fig. 2a and Fig. S4) does not permit the proper

deconvolution of the kinetics of these processes (further experiments aiming more accurately to analyze the kinetics are in progress); however, some general remarks are still possible.

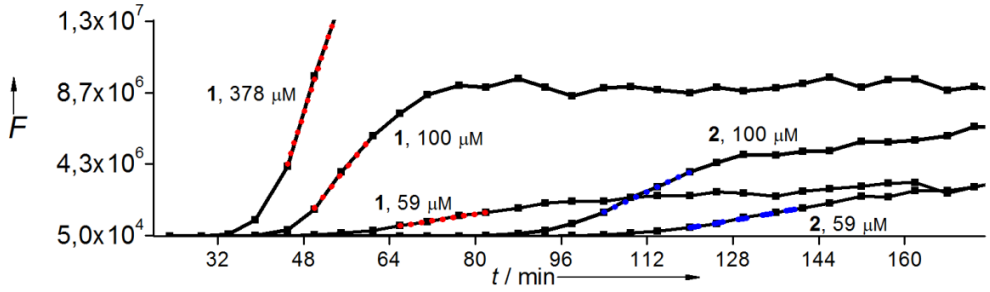

Fig. S4 Detail of the fluorescence signals obtained during the initial stages of the kinetic experiments, plotted with a linear vertical axis. Red (probe **1**) and blue (probe **2**) dotted lines indicate the linear fits giving m_{max} as discussed below.

(a) The signal plateaux reached in the experiment can be assumed to indicate total activation of the initial quantity of the probes. Fluorescence signals from probes **1** and **2** at identical concentrations show almost identical plateau values, suggesting that both diastereomers of 1 are enzymatically hydrolyzed. Furthermore, both diastereomers of 1 appear to be hydrolysed at comparable rates, since otherwise Fig.s 2a and S4 would display two disctinct regions: faster hydrolysis of one diastereomer, then slower action on the other, whereas the signal is in fact smoothly sigmoidal.

(b) The lag time t_{lag} between the start of the experiment and the observation of a definite fluorescence signal is clearly visible in all cases, and t_{lag} increases as the initial substrate concentration decreases. After this period, the fluorescence signal adopts a sigmoidal-shaped curve, *i.e.* after a further time (around 10 minutes) the signal as a function of time reaches a maximal gradient m_{max} which is kept roughly constant over a period of no less than 20 minutes, before signal increase begins to slow, and the signal gradually attains the plateau value. Due to data scattering, the time $t_{1/2}$ when the signal reaches half of its plateau value is more easily determined than a time when the plateau value itself is reached. For all the signals examined, the region of signal displaying m_{max} also contained the datapoint corresponding to $t_{1/2}$. A table of values of t_{lag}, m_{max}, and $t_{1/2}$ for the higher-concentration experiments where the signal plateaux could more reliably be determined is given as Table S3. Errors of around 20% are to be expected in these data, as only one data point was acquired every 5.5 minutes, requiring judicious fitting.

Table S3 Values of the observed lag times before signal generation began (t_{lag}), maximal gradient of signal generation (m_{max}), times for half the plateau signal value to be generated ($t_{1/2}$).

Probe Series	t_{lag} (min)	m_{max} ($\times 10^4$ RFU/min)	$t_{1/2}$ (min)
1, 378 μM	≤23	100	57
1, 100 μM	34	40	57
2, 100 μM	77	15	125
1, 59 μM	39	5.1	90
2, 59 μM	88	5.7	146

(c) The lag times for probe **2** are approximately double that of probe **1** when their concentrations are kept equal. This implies either slower cyclisation, or slower enzymatic processing (or both) of **2** than of **1**.

(d) Considering the three-step kinetics, it can be seen that the values $t_{1/2}$ obtained from the fluorescence signals represent upper bounds for the halftimes of cyclisation, t_{cyc}, as these values also contain contributions from the rate of enzymatic hydrolysis (this cannot simply be calculated from the 'units' reported by the enzyme supplier as these refer to a different substrate and to different conditions; see **Enzymatic Testing Procedure**), and also from the time t_{lag} needed to supersaturate the solution and commence nucleation and thus signal generation. This time t_{lag} is highly significant, on the order of half of the obtained values of $t_{1/2}$. While the data do not permit us to deconvolute the enzyme hydrolysis and cyclisation steps, a first approximation to 'removing' the influence of t_{lag} from the initial upper bound $t_{cyc} \leq t_{1/2}$ would therefore be to simply subtract t_{lag}. Cyclisation should be a first-order process, therefore it would be expected that t_{cyc} would be a constant for each probe, regardless of its concentration, thus permitting us to give modified halflives for the two-step procedure (enzymatic hydrolysis + cyclisation) as 23 min for probe **1** and 48 min for probe **2** (i.e. these are the modified upper bounds for t_{cyc} that can be given based on this experimental data) based on the values calculated for their 100 μM concentrations. It would not be unconceivable that the true cyclisation halftime, once deconvoluted from the enzymatic hydrolysis, would be substantially less than this figure. It is worthwhile comparing these upper bounds to the cyclisation halftimes reported at the higher temperature of 37°C for 1,2-diamine based but non-preorganised spacers: an N'-methyl (thus substantially more nucleophilic than the present primary amines, but unsuitable for general application to peptidases) derivative was reported to have a halflife of 36 minutes, whereas its unsubstituted primary amine analogue had a halflife of 304 minutes.[S11] Although as stated above further quantification of the kinetics of these spacers is necessary, the power of the preorganisation of these spacers is evident in the fact that *even when their cyclisation kinetics are*

convoluted with a preceding reaction of enzymatic hydrolysis, they perform similarly or better than non-preorganized, but more nucleophilic spacers which are merely cyclising in a single step!

It should also be noted (Fig. 2b) that while the signal values for the controls of **2** are, pleasingly, concentration-independent, those for **1** are five times higher for its 100 μM control than for its 10 μM control, even though both are stable. One possible factor is that the kinetic test whose results were presented here used a *p*-TsO^- counterion for probe **1** whereas a TFA counterion was used for probe **2**. It was observed in the solid state that the *p*-TsOH salt of **1** gave a far stronger (yet strictly blue) fluorescence than its TFA salt; it is possible that this fluorescence was due to the *p*-TsO^- counterion, and that it may have retained some of this fluorescence activity in solution, leading to the observed increase in the solution-state fluorescence with its increasing concentration.

Towards an Enzyme Activity Detection Limit

Research concerned with probes operating on an increase in fluorescence after enzymatic activation commonly cites a 'detection limit' for the protein targeted, which is a function of the ratio between control and active fluorescence signals. In this case, as we have discussed (references 2-4 and the first paragraph of the main text, plus discussion on pages S16 and S22-S23), the situation is altogether different: the principle of a true binary off-ON system is to give an *arbitrarily low* detection limit for enzyme activity, by allowing longer incubation to compensate for lower activity without any false positive signal masking the results. Our system provides the first demonstration of such a fluorogenic aminopeptidase probe.

Detection is therefore achieved as soon as the released fluorophore concentration (dependent on the protein activity used, the rate of substrate processing, and initial probe concentration) passes the nucleation threshold specific to that fluorophore (dependant also on the temperature, pH, other dissolved species, etc) and the fluorescence passes the signal-to-noise threshold of the fluorimeter setup used (dependant on the acquisition settings, the machine, the cleanliness of the microplate, the purity of the probe sample used in the experiment, etc). Therefore a 'detection limit' will be a function of all these parameters, as well as of the time allowed for the experiment. A detection limit using this model aminopeptidase and model fluorophore in a model setting would not be transferable once any of these parameters are changed, so will not necessarily

provide useful extra numerical information to the reader interested in applying this novel, binary off-ON system to *eg.* prodrug design, let alone to probes constructed with any other substrate, or using any other protease type or concentration, type of fluorophore, temperature, pH, test media conditions, or detection protocol.

What *can* be transferred to any application, is that our system delivers, for the first time, the promise of an *arbitrarily low detection limit* (in the context of probe design; of course, for applications to *eg.* prodrugs, such a figure is not meaningful) which will depend exclusively on the nature of the application and implementation (choice of the parameters listed above, notably, fluorophore and test media conditions, protein activity, and probe concentration). We therefore consider that determining a detection limit for the model system we currently report misses the greater, conceptual importance of the information we already supply, and risks even obscuring the capabilities of our system. However we give a brief sample calculation as follows, keeping in mind that (as we discussed on pages S15-S16), while protein activity depends on a complex set of factors, we *already* chose our protease concentration to be among the lowest used in the literature we have seen, being for example five hundred times lower than that used in reference S7. The fact that our probes generate signal in around only ten minutes with this low LAP protein activity already highlights the excellent sensitivity of our system; a sample 'detection limit' we can calculate serves only to reinforce this conclusion, but should not form the exclusive basis of evaluation and comparison of our probe system with conceptually different, prior art systems.

If we consider an initial probe **1** concentration of ~200 μM used in a twenty-four-hour incubation with our described experimental parameters, we can be sure that no false positive background signal will arise (see Results: Scanning Tests). We have calculated a solubility threshold for the model fluorophore HPQ in our conditions as 5.7 μM (see Results: Kinetic Tests), so detection will be achieved when more than 5.7 μM of probe is processed in 24 hours: to be firmly 'on the safe side' we might require 12 μM to be processed (ie more than double the minimum amount) to count as a highly reliable detection; this would deliver a fluorescence signal of *ten times* the *total* background fluorescence signal of a blank sample (Table S2) *without requiring the subtraction of background spectra*. We can calculate a *minimum estimate, v**, for the rate of processing of the probe by LAP when the LAP concentration is small (and *v** will likely be significantly less than the true v_{max}: see below) by examining the initial rate of processing determined for the Kinetic Tests. Table S2 showed that each 1 μM of precipitated

fluorophore gave approximately 10^5 RFU in those conditions; and with that protein concentration of ~3.5 μgmL^{-1} (~60 nM[S9]), m_{max} for a 200 μM experiment would lie between 40×10^4 and 100×10^4 RFU/min (100 μM and 378 μM experiments, respectively: see Table S3. It can therefore be noted too, that the 60 nM of enzyme was *not* saturated at 100 μM probe concentration). If we postulate a conservative estimate of m_{max} for a (200 μM probe, 60 nM peptidase) experiment as 60×10^4 RFU/min, we therefore have a maximal (ie. nearest to peptidase-saturation conditions) probe processing rate of $\boldsymbol{v^*}$ **= 0.1 μM probe per minute per nanomolar of peptidase**. If we decrease the peptidase concentration, the peptidase will approach more closely true saturation conditions, ie, v^* will increase – possibly, greatly increase - to approach the true v_{max} which would be seen with a large probe concentration (200 μM) relative to the 'detection-limit amount' of peptidase with this probe and detection parameters. Combining this minimum estimate for the processing velocity with the 12 μM processed probe we required as an overestimate for the detection threshold after 24 hours' incubation, gives a conservative underestimation of the actual probe's detection limit as **80 pM of leucine aminopeptidase.** In terms of this peptidase's activity upon our substrate, this can also be expressed as 0.012 μmol probe conversion per mL per 24 hours, *ie.* **8×10^{-6} UmL^{-1} of leucine aminopeptidase.** We stress however, that this is a vast underestimation of the optimised detection limit of the probe system, in two respects: firstly, as regards the stringent requirements and conservative estimations employed during this calculation, as well as the non-optimal pH and temperature used; and secondly, as regards the true possibilities of our system as applied to other fluorophores, chiefly those with a lower nucleation threshold. For example, addressing only the second point, using a fluorophore of similar brightness but with an 0.5 μM solubility limit under similar circumstances, would give a conservative detection limit on the order of 1×10^{-6} UmL^{-1}. We repeat however that this figure – which we still feel to be underestimates – are only indications of the sort of performance that can be expected from our system; the true novelty it provides is not a mere gradual increase, but instead a leap into a new regime, of detection sensitivity and reliability: true binary, off-ON performance.

Abbreviations

Boc : *tert*-butoxycarbonyl

BocLeuOH : *N*-*tert*-butoxycarbonyl- L-leucine

Cy : cyclohexane

DCC : 1,3-dicyclohexyl-carbodiimide

DCM : dichloromethane

DCU : 1,3-dicyclohexylurea

DDQ : 2,3-dichloro-5,6-dicyano-1,4-benzoquinone

DMSO : dimethylsulfoxide

EA : ethyl acetate

HPQO-H (≡HPQ) : 2-(2-hydroxyphenyl)quinazolin-4(3*H*)-one

HPQO- : 2-(4-oxo-3,4-dihydroquinazolin-2-yl)phenoxy

LeuOH : L-leucine

LAP : Porcine Liver Leucine Aminopeptidase, EC 3.4.11.1

p-TsOH : *para*-toluenesulfonic acid

RFU : Random Fluorescence Units

RT : room temperature (~22-26°C)

sat. : a saturated aqueous solution of

spont. : spontaneous

TFA : trifluoroacetic acid / trifluoroacetate

THF : tetrahydrofuran

Tris : 2-hydroxymethyl-2-amino-1,3-propanediol

NMR Appendix

7: ^{1}H-NMR and ^{13}C-NMR spectra

7: ^{1}H-NMR spectrum (200 MHz, $CDCl_3$)

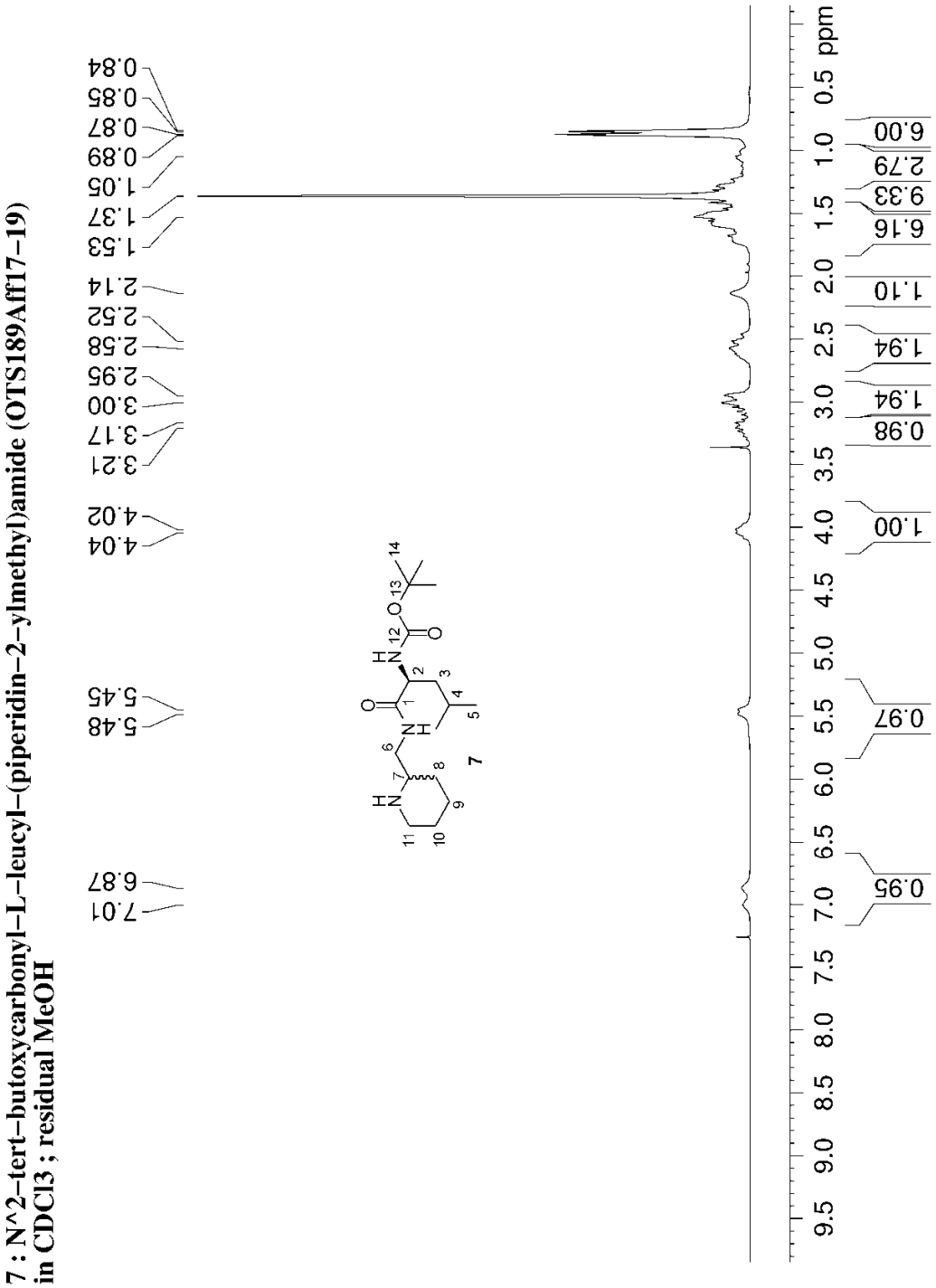

7: ^{13}C-NMR spectrum (50 MHz, $CDCl_3$)

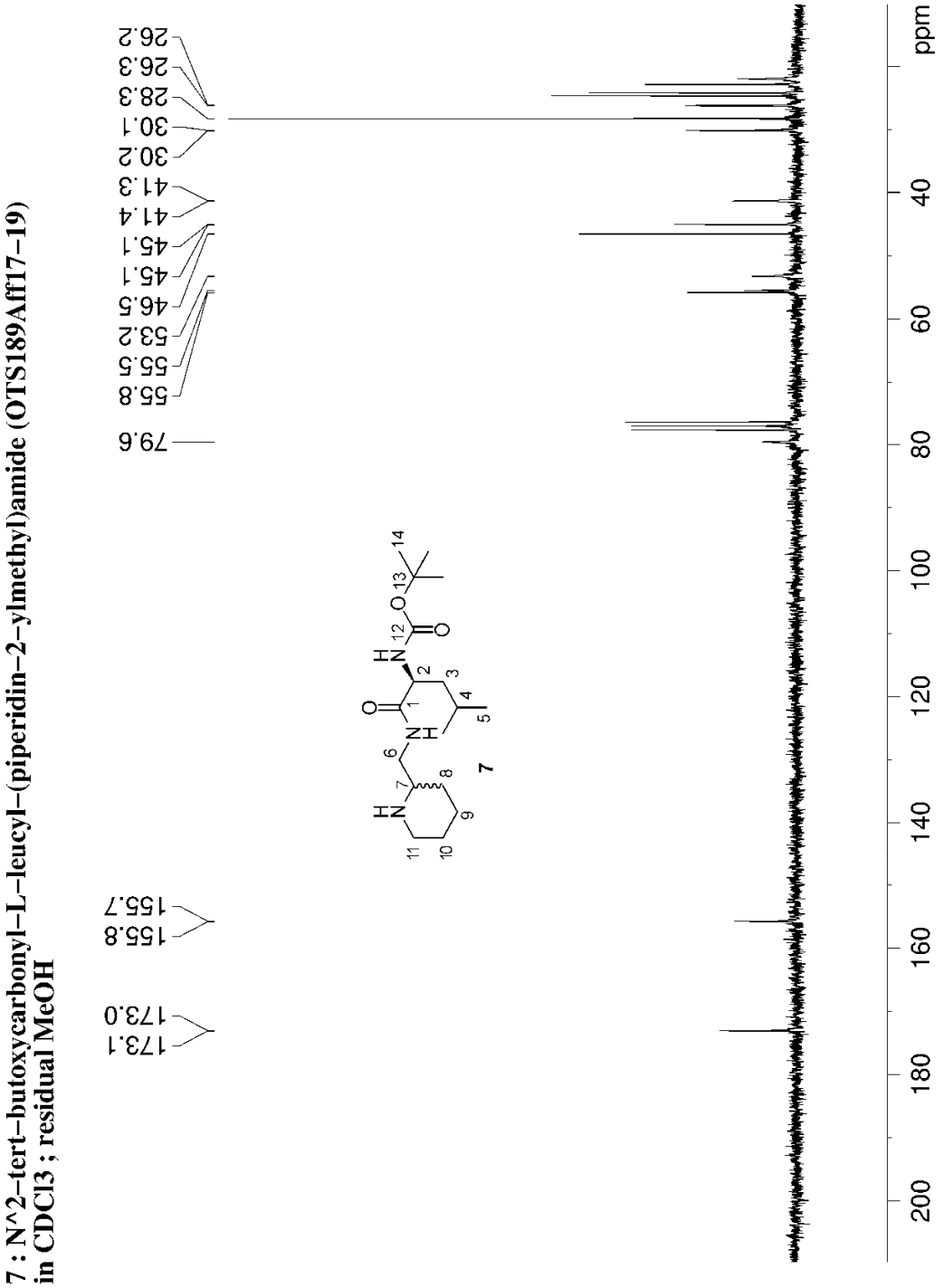

S1: ^{1}H-NMR spectrum

S1: ^{1}H-NMR spectrum (200 MHz, $CDCl_3$)

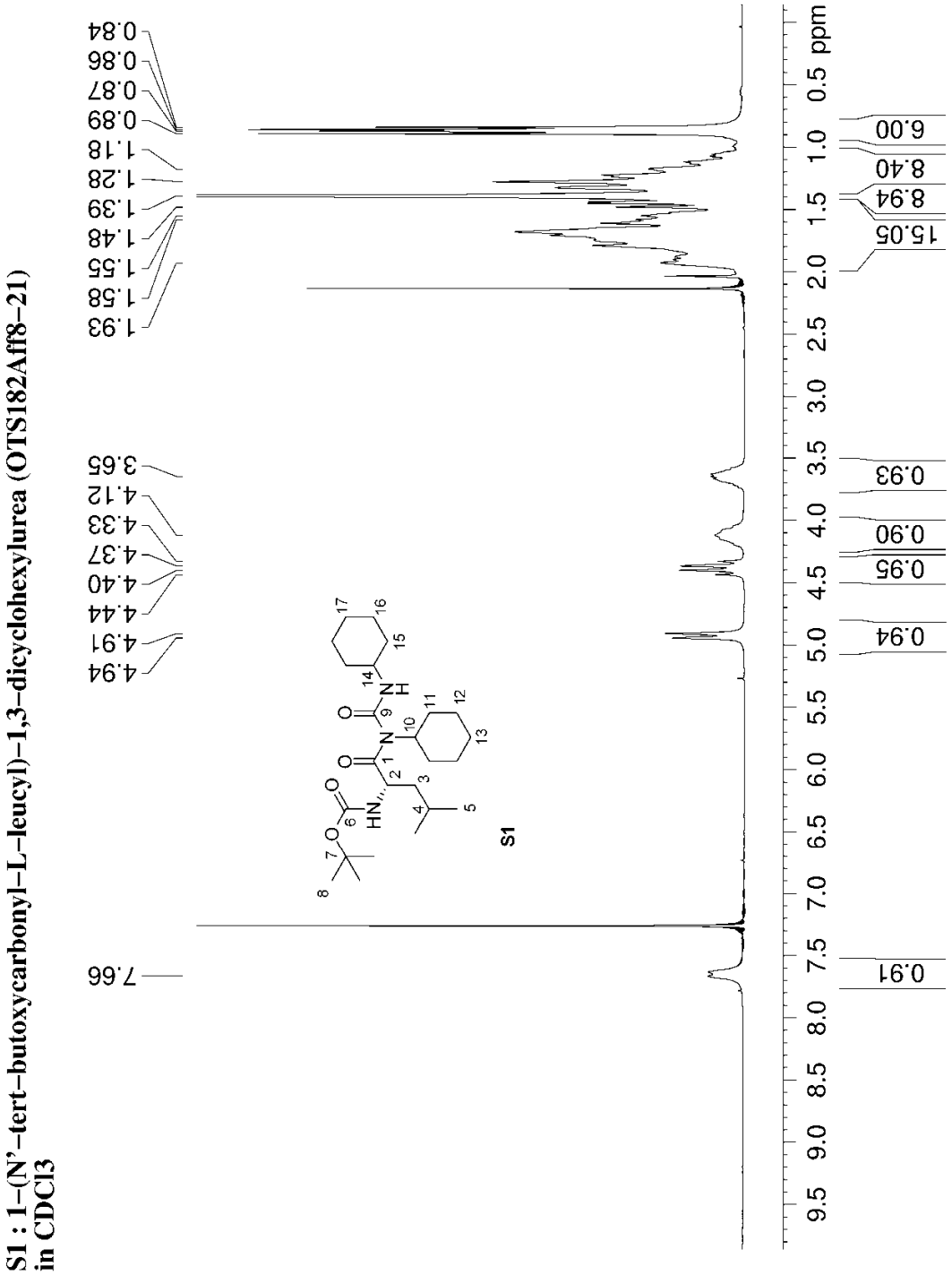

9: ^{1}H-NMR spectrum

9: ^{1}H-NMR spectrum (500 MHz, $CDCl_3$)

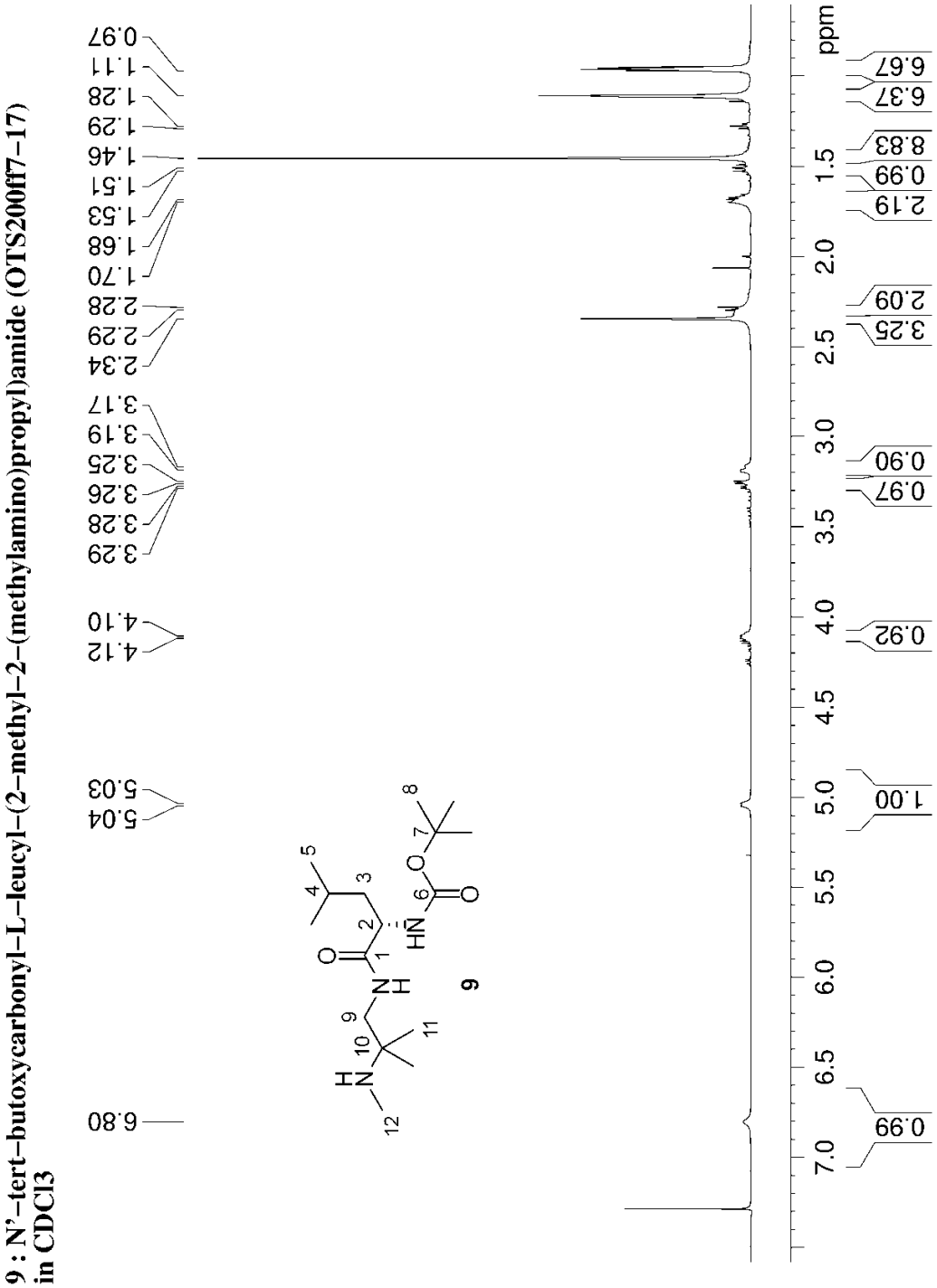

S4: ^{1}H-NMR and ^{13}C-NMR spectra

S4: ^{1}H-NMR spectrum (500 MHz, $CDCl_3$)

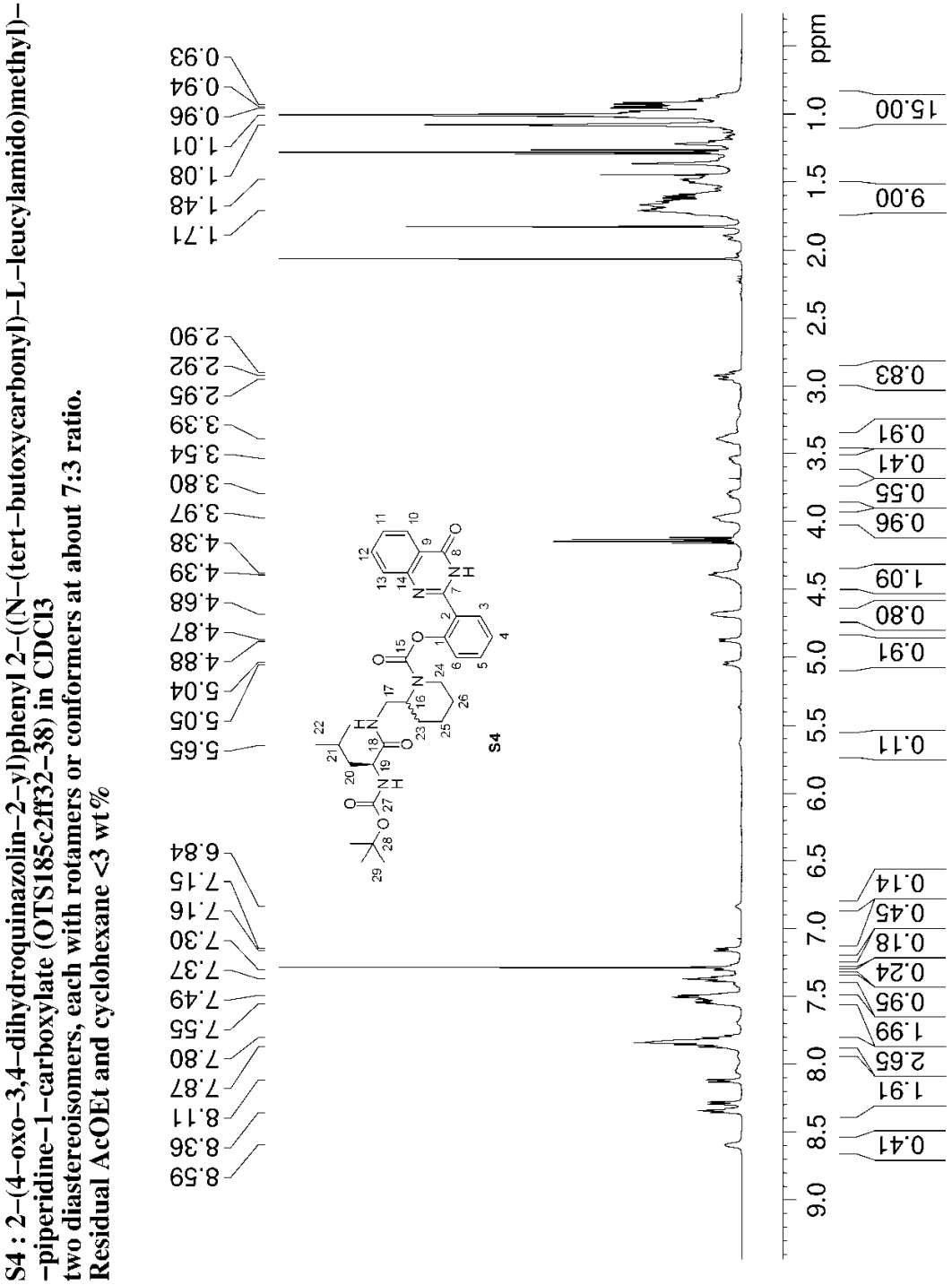

S4: ^{13}C-NMR spectrum (125 MHz, $CDCl_3$)

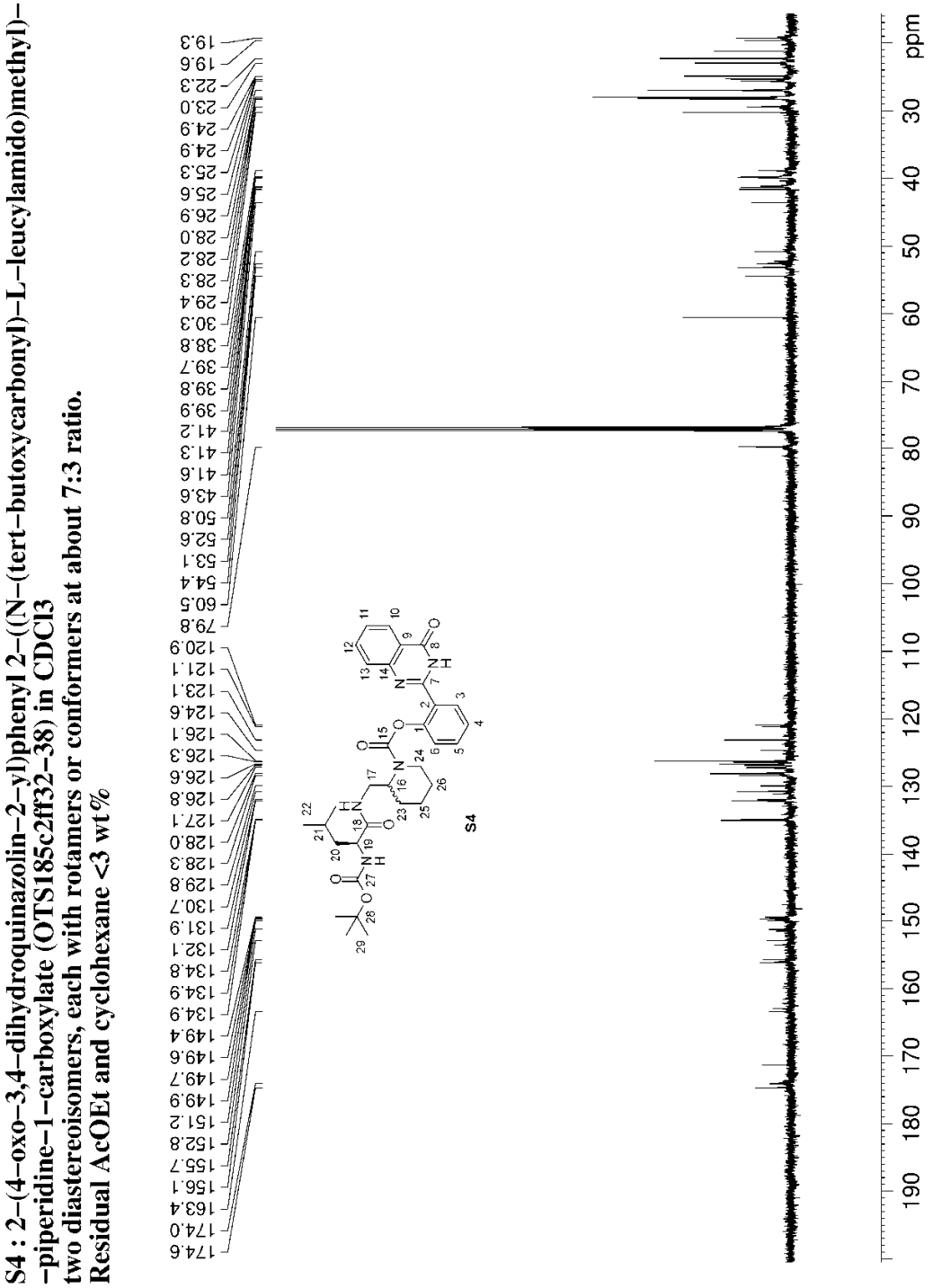

S5: ^{1}H-NMR and ^{13}C-NMR spectra

S5: ^{1}H-NMR spectrum (500 MHz, $CDCl_3$)

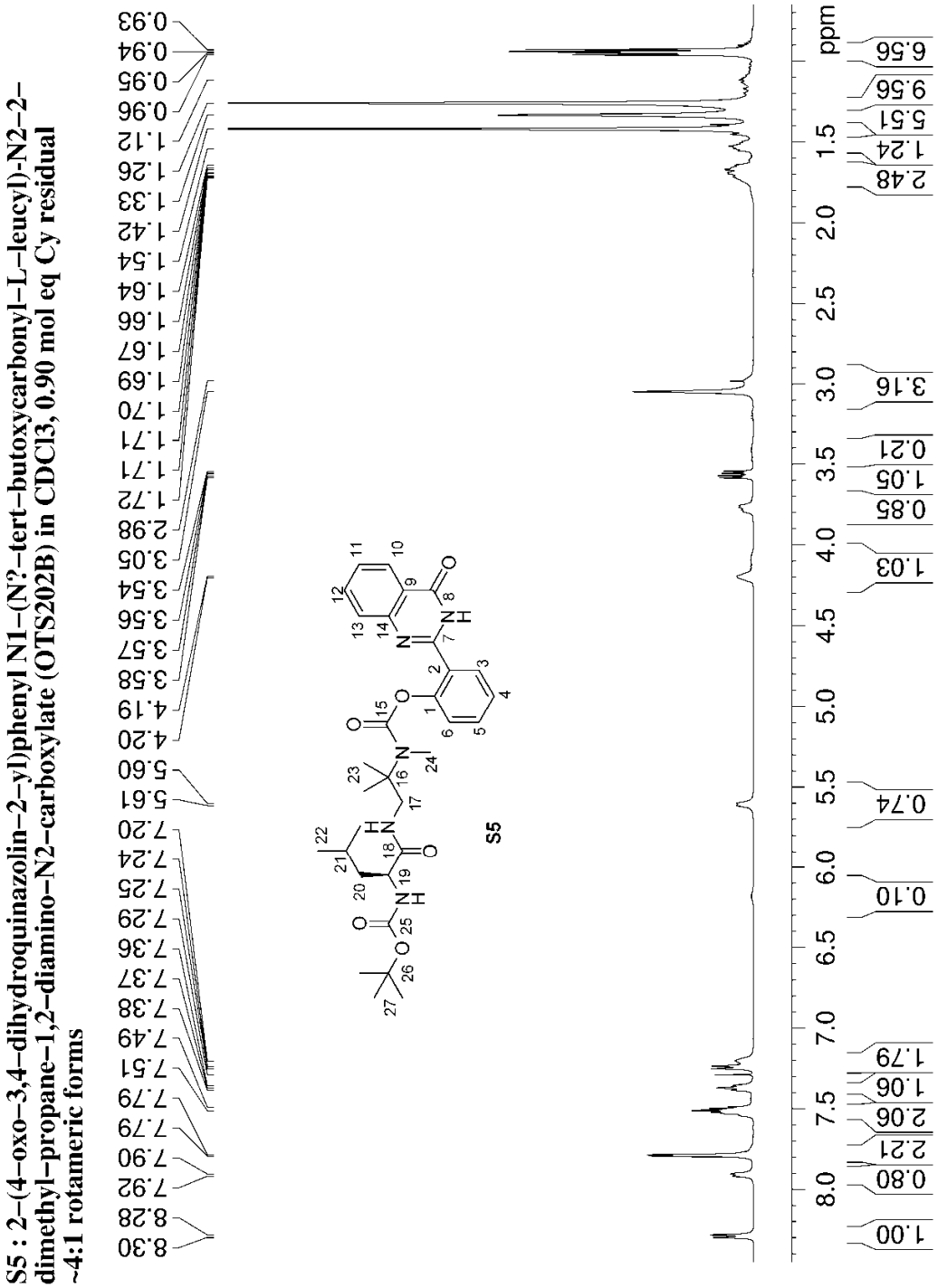

S5: ^{13}C-NMR spectrum (125 MHz, $CDCl_3$)

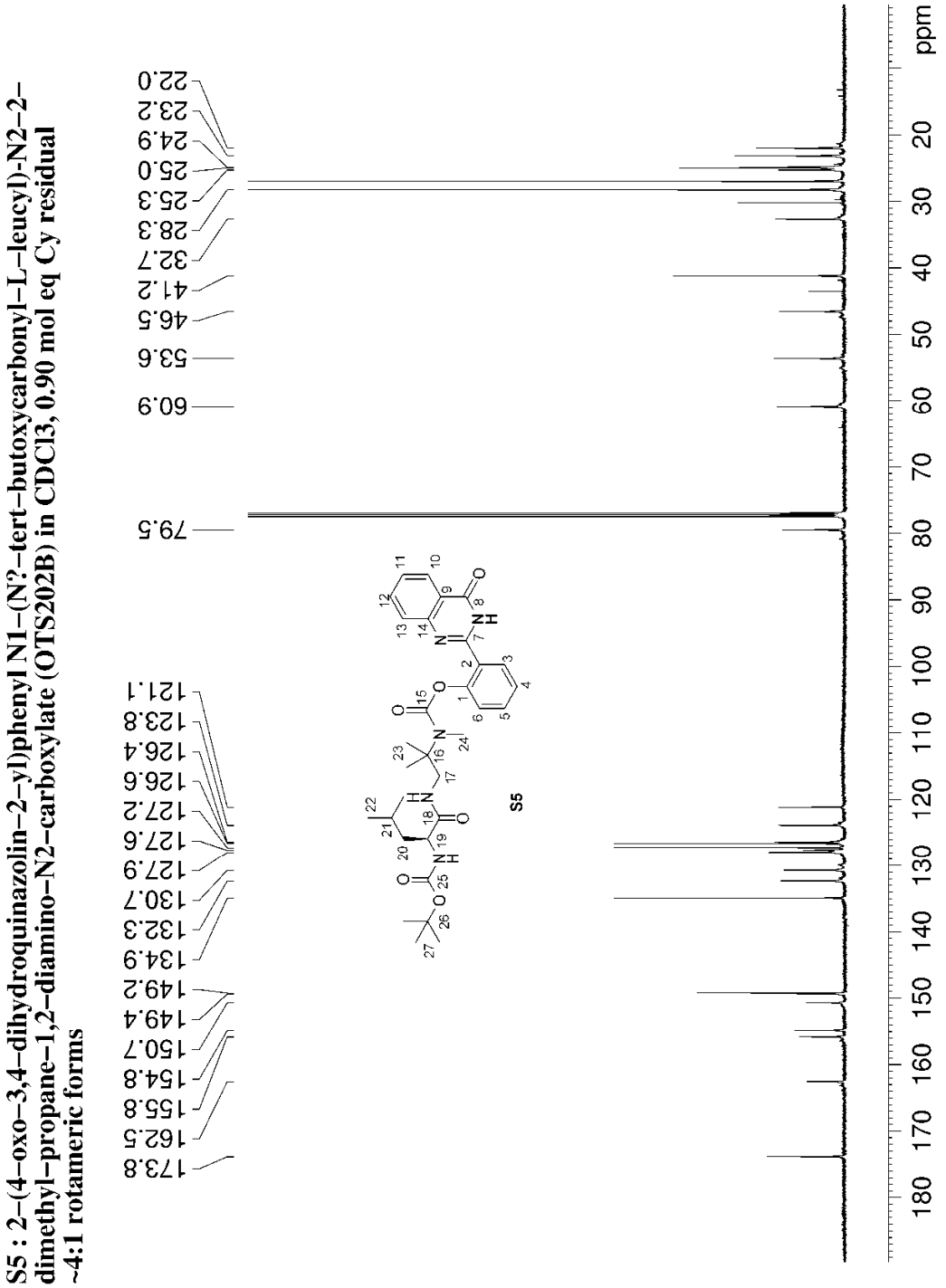

1: ^{1}H-NMR and ^{13}C-NMR spectra

1: ^{1}H-NMR spectrum (500 MHz, D_2O, TFA counterion)

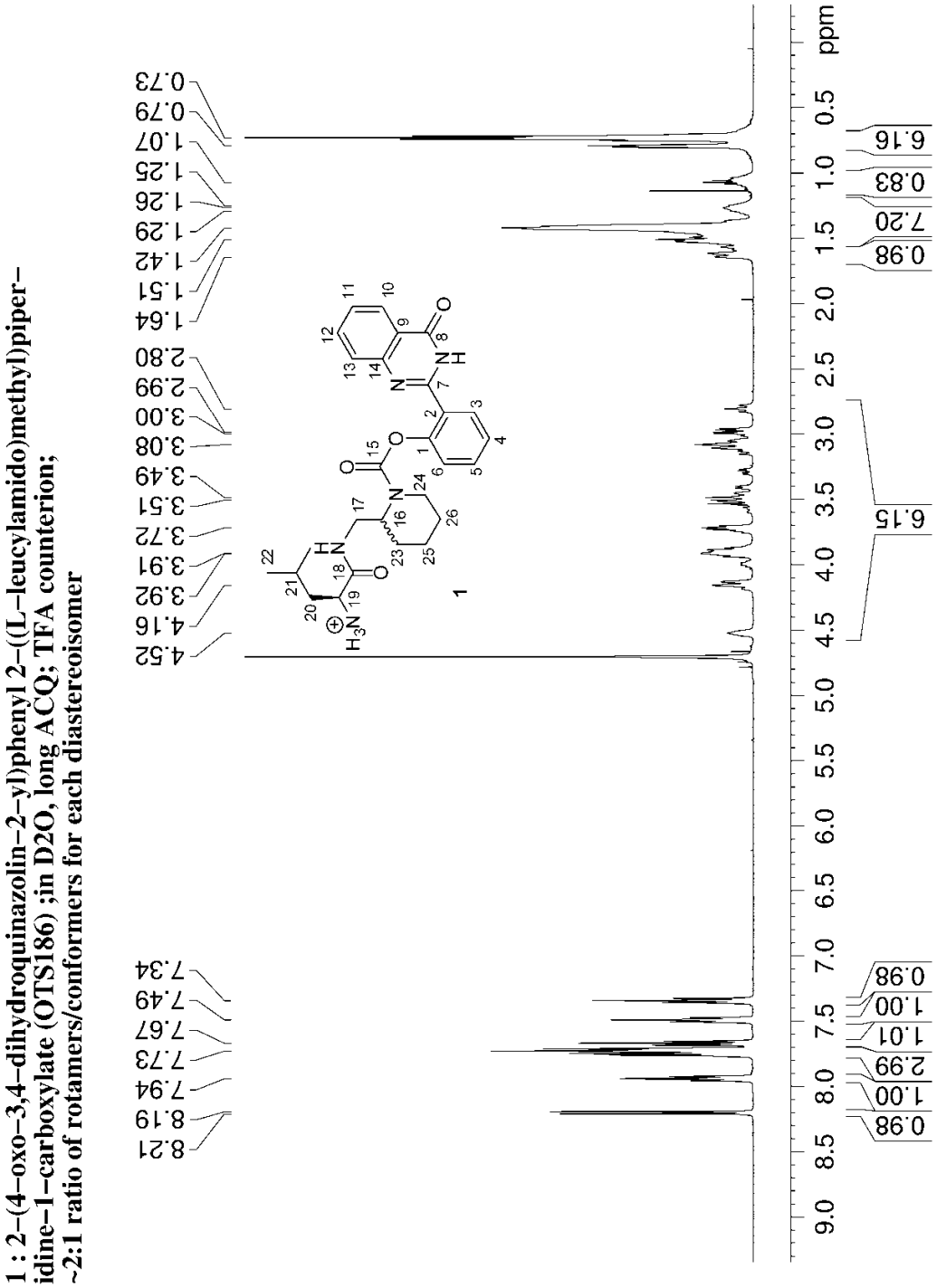

1: ^{13}C-NMR spectrum (125 MHz, D_2O, TFA counterion)

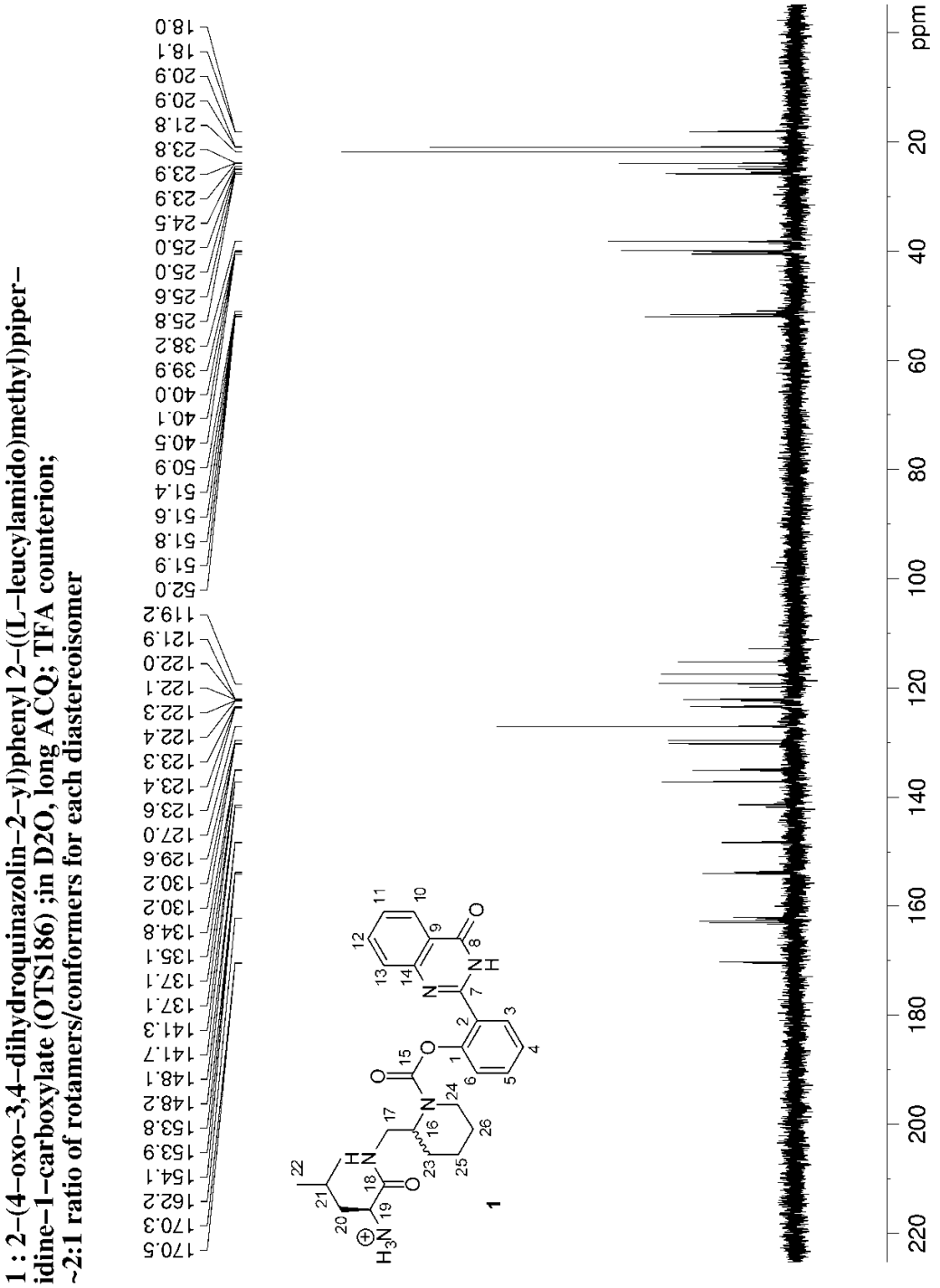

2: ^{1}H-NMR, ^{13}C-NMR and udeft spectra

2: ^{1}H-NMR spectrum (500 MHz, D_2O, TFA counterion)

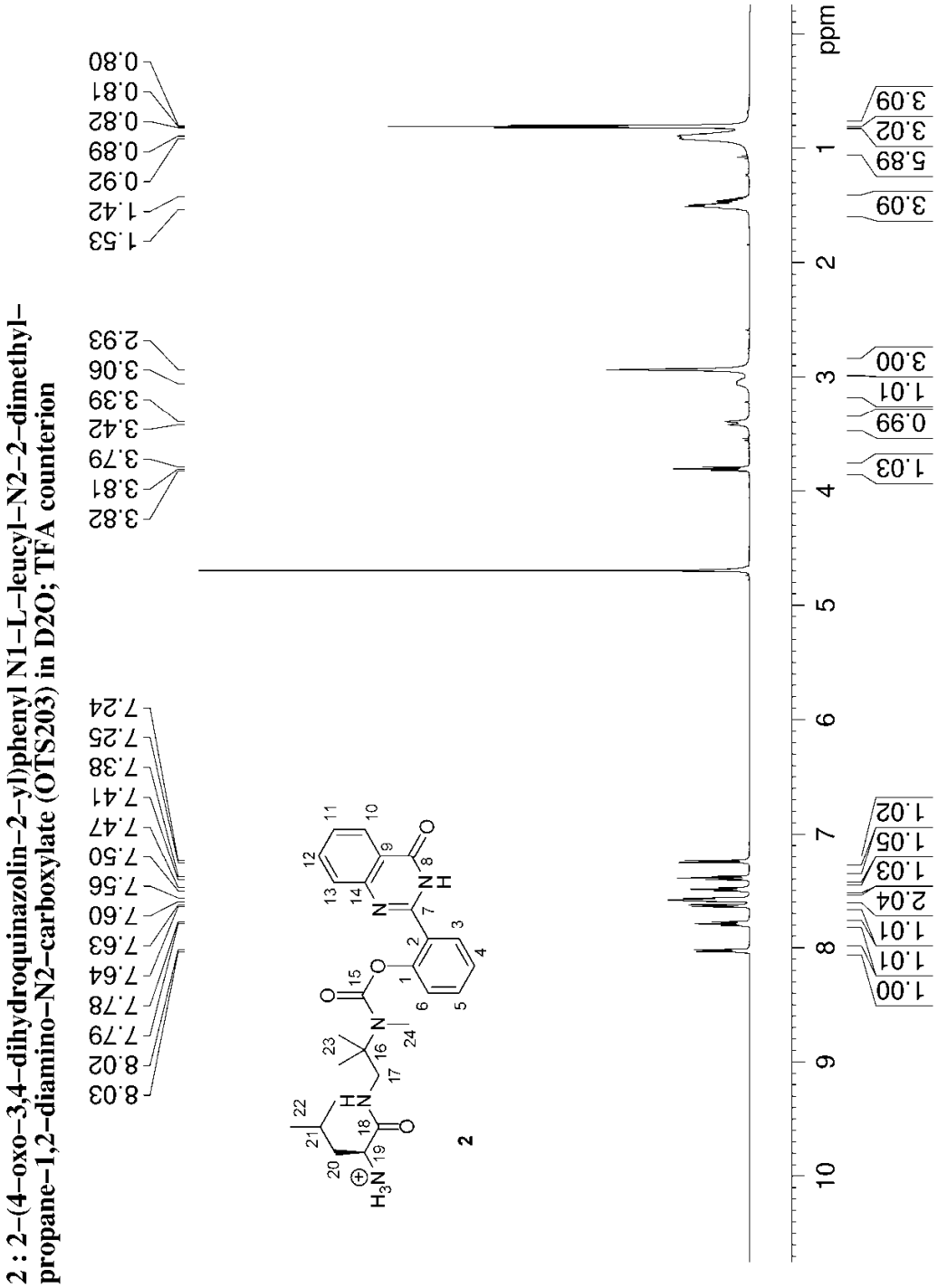

2: ^{13}C-NMR spectrum (125 MHz, D_2O, TFA counterion)

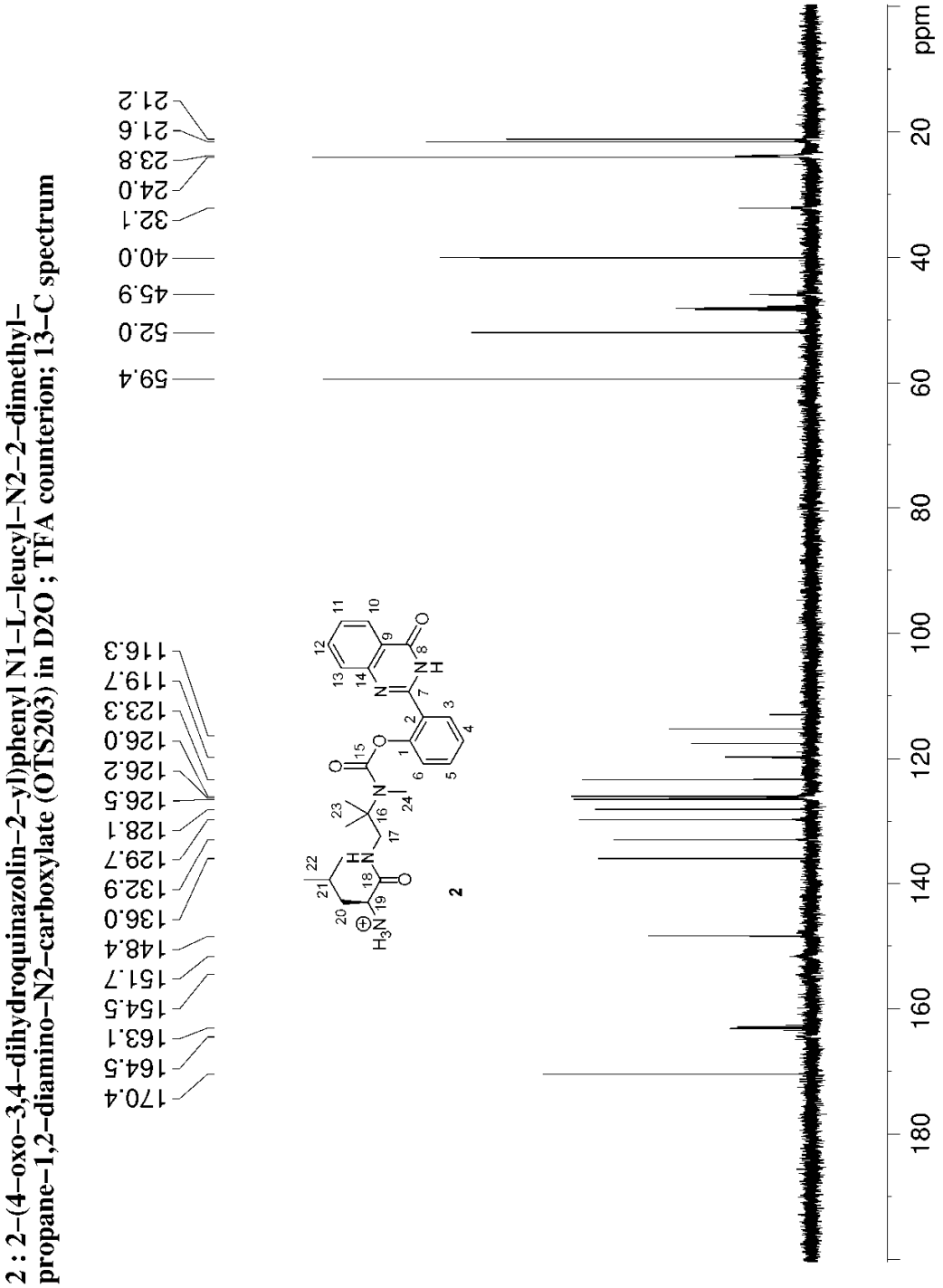

2: udeft ^{13}C-NMR spectrum (125 MHz, D_2O, TFA counterion)

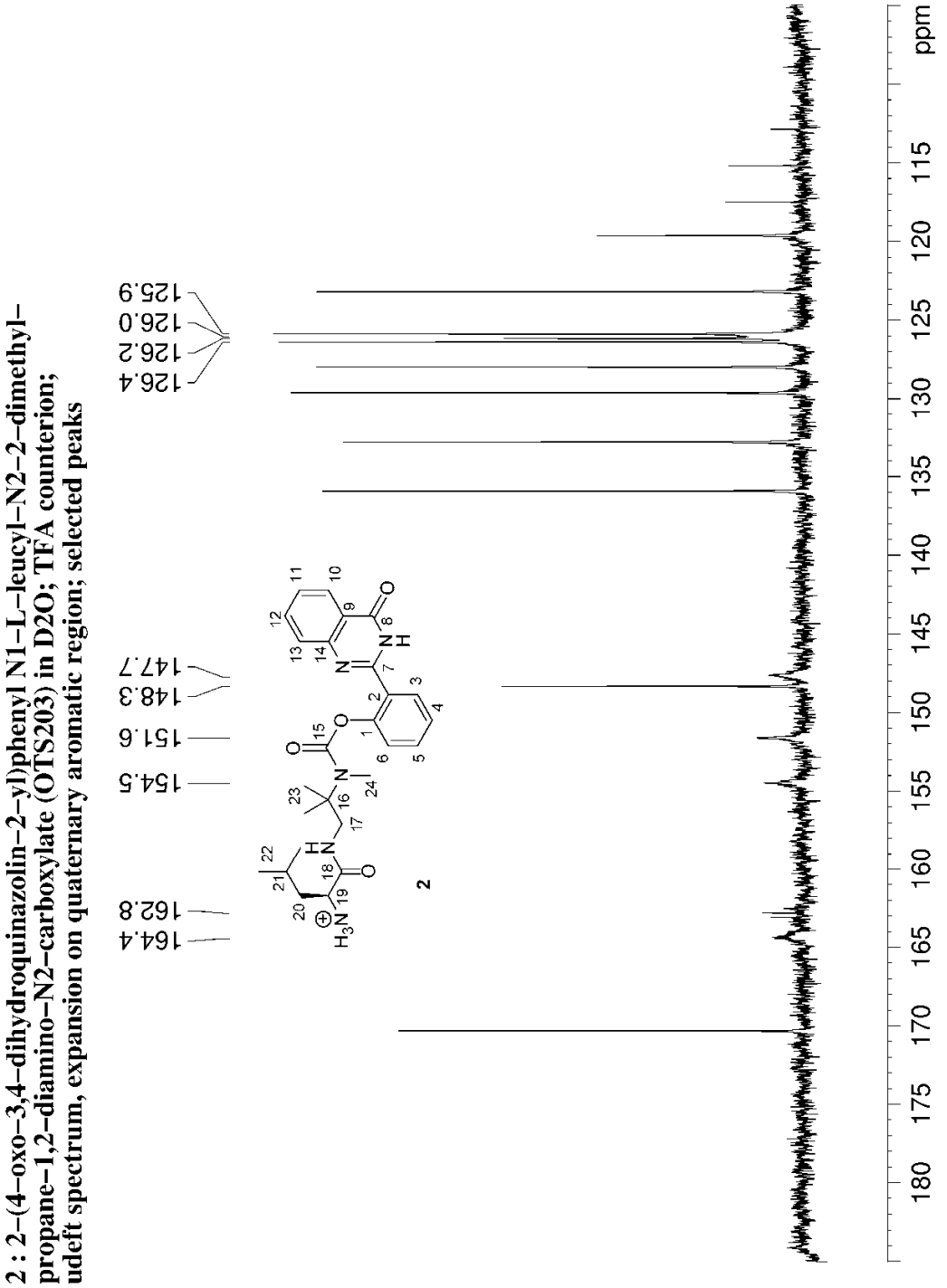

Electronic Supplementary Information Bibliography

S1 M. Waibel, Ph.D. Thesis, Ecole Normale Supérieure de Lyon, 2009.

S2 M. Baghbanzadeh, M. Dabiri and P. Salehi, *Heterocycles*, 2008, **75**, 2809-2815.

S3 K. Faghihi, K. Zamani, A. Mirsamie and M. Reza Sangi, *Eur. Polym. J.*, 2003, **39**, 247-254.

S4 L. J. Exner, L. S. Luskin and P. L. de Benneville, *J. Am. Chem. Soc.*, 1953, **75**, 4841-4842.

S5 *US Pat.*, 20050038078, 2005.

S6 M. Piotto, M. Bourdonneau, K. Elbayed, J.-M. Wieruszeski and G. Lippens, *Magn. Reson. Chem.*, 2006, **44**, 943-947.

S7 M. Kamiya, D. Asanuma, E. Kuranaga, A. Takeishi, M. Sakabe, M. Miura, T. Nagano and Y. Urano, *J. Am. Chem. Soc.*, 2011, **133**, 12960-12963.

S8 R. E. Beattie, D. J. Guthrie, D. T. Elmore, C. H. Williams and B. Walker, *Biochem. J.*, 1987, **242**, 281-283.

S9 O. Vincent-Fiquet, J. C. Rogez and R. Plaquet, *Biochimie*, 1984, **66**, 171-174.

S10 V. B. Paragas, J. A. Kramer, C. Fox, R. P. Haugland and V. L. Singer, *J. Microsc.*, 2002, **206**, 106-119.

S11 W. S. Saari, J. E. Schwering, P. A. Lyle, S. J. Smith and E. L. Engelhardt, *J. Med. Chem.*, 1990, **33**, 97-101.